Solar Energy Materials and Solar Cells 187 (2018) 39–54

Contents lists available at ScienceDirect

Solar Energy Materials and Solar Cells

journal homepage: www.elsevier.com/locate/solmat

Surface passivation of crystalline silicon solar cells: Present and future

Jan Schmidt[a,b,*], Robby Peibst[a,c], Rolf Brendel[a,b]

[a] Institute for Solar Energy Research Hamelin (ISFH), Am Ohrberg 1, 31860 Emmerthal, Germany
[b] Department of Solar Energy, Institute of Solid-State Physics, Leibniz Universität Hannover, Appelstr. 2, 30167 Hannover, Germany
[c] Institute for Electronic Materials and Devices, Leibniz Universität Hannover, Schneiderberg 32, Germany

ARTICLE INFO

Keywords:
Silicon solar cells
Surface passivation
Carrier-selective contacts

ABSTRACT

In the first part of this paper, we review the developments which led to the present state-of-the-art in the surface passivation of today's industrially predominant dopant-diffused crystalline silicon (c-Si) solar cells, based on dielectric layers such as silicon oxide, silicon nitride, aluminum oxide and stacks thereof. In the second part of this review, we focus on the future developments in the field of c-Si solar cells based on carrier-selective passivation layers. Whereas the dielectric layers are insulating and are hence applied only for passivating the non-contacted areas of the silicon surface, the carrier-selective passivation layers are intended to provide an effective passivation of non-contacted as well as contacted areas of a c-Si solar cell, thereby increasing the efficiency potential of c-Si solar cells significantly. Due to the fact that the carrier-selective layers are implemented in a contact, besides the good passivation properties for minorities, these layers must also provide a good majority carrier transport, i.e. they have to provide a low contact resistance. Both properties, i.e. suppression of minority-carrier recombination as well as good majority-carrier transport, define the selectivity of the carrier-selective contact, which is an important figure of merit for the assessment and comparison of different types of carrier-selective contacts. One very promising type of carrier-selective passivation layer is based on heavily doped polycrystalline silicon layers deposited on a thin silicon oxide layer, the latter providing the excellent passivation while enabling efficient majority-carrier transport via pin-holes and/or tunneling. Moreover, we discuss metal oxides and conductive polymers, which have only recently been applied to c-Si photovoltaics, but seem to have a promising potential as low-cost selective contact materials. We finally compare combinations of the various options of carrier-selective layers concerning their combined selectivities and efficiency potentials.

1. Introduction

The steadily increasing bulk carrier lifetimes of crystalline silicon (c-Si) wafers for the application to commercial c-Si solar cells makes recombination at the cell surfaces and at the contacts the major fundamental limitation in today's c-Si solar cells. This review on surface passivation starts with describing the developments that led to today's level of surface passivation by means of dielectric layers in state-of-the-art industrial passivated emitter and rear cells (PERCs) and then describes future options based on alternative passivation layer materials that are carrier-selective and allow for a good majority-carrier transport as well as an excellent blocking of minority carriers.

Fig. 1 shows a schematic of a PERC-type c-Si solar cell, as it is produced today in industry on *p*-type c-Si wafers in different versions, such as monofacial or bifacial (the latter shown in Fig. 1). The c-Si wafer absorbs solar photons and the light-generated electrons flow towards and through the phosphorus-diffused n^+ emitter (acting as an electron-selective region) to reach the screen-printed silver (Ag) grid. The holes flow through a locally formed aluminum-doped p^+ back surface field (acting as a hole-selective region) to the screen-printed aluminum (Al) contact. The front metallization on the n^+ emitter covers only a small area fraction (typically between 2% and 5%) to keep the shadowing and the recombination losses at the metal/c-Si contact as small as possible. The larger rest of the front surface area is coated with a dielectric layer of silicon nitride (SiN_x), simultaneously acting as effective surface passivation and antireflection coating. The rear side metallization on the p^+ region has an area fraction of typically 5–20% that is larger than the metallization fraction at the front due to the use of cost-effective Al screen-printing technology. The larger fraction of the rear surface (80–95%) is passivated by dielectric layer stacks, where Al_2O_3/SiN_x stacks have proven to be most effective in commercial screen-printed cells. This review discusses the four types of surfaces that appear in Fig. 1: (i) The dielectric passivation of the dopant-diffused c-Si surface (at A in Fig. 1), (ii) the passivation of the non-

* Corresponding author at: Institute for Solar Energy Research Hamelin (ISFH), Am Ohrberg 1, 31860 Emmerthal, Germany.
E-mail address: j.schmidt@isfh.de (J. Schmidt).

https://doi.org/10.1016/j.solmat.2018.06.047
Received 11 January 2018; Received in revised form 25 May 2018; Accepted 25 June 2018
Available online 27 July 2018
0927-0248/

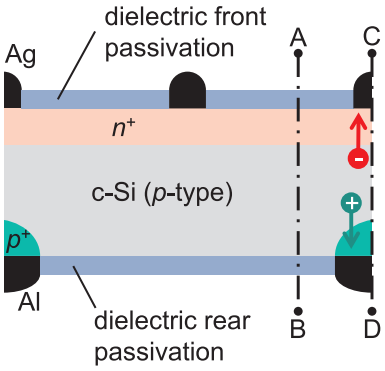

Fig. 1. Schematic of a PERC-type silicon solar cell; the front-side texture is not shown. The band diagrams along the lines A-B and C-D are illustrated in Figs. 3 and 7, respectively.

diffused c-Si surface (point B), as well as (iii) the passivation of contacts with a dopant-diffused electron-selective region (point C) and (iv) the passivation of the metal contacts by a doped hole-selective region (point D). In addition, we also discuss the dielectric passivation of boron-diffused p^+ hole-selective regions, applied in today's commercial solar cells on n-type c-Si material.

In the second part of this paper, we review several materials that provide an improved contact passivation in comparison to the implementation of dopant-diffused n^+ and p^+ regions, as used in most of today's industrial solar cells. These electron- and hole-selective layers largely suppress contact recombination and, at the same time, allow for an effective transport of the majority carriers to the metal contacts. Fig. 2 shows schematics of two different versions of solar cells featuring carrier-selective layers: (a) a both-sides-contacted and (b) a rear-side-contacted cell. Due to the fact that the carrier-selective layers mostly not provide a sufficiently high lateral conductivity, in the case of both-sides-contacted cells they typically require a full-area conducting layer on top, such as a transparent conductive oxide (TCO), in order to transport the carriers to the front metal fingers. Note that the both-sides-contacted cell structure shown in Fig. 2(a) is technologically relatively simple to process due to the omission of complex structuring steps. On the other hand, due to absorption losses in the front TCO layer, the rear-contacted cell structure shown in Fig. 2(b) has a higher short-circuit current and hence efficiency potential, coming however at the cost of an increased process complexity. The TCO layers at the rear are optional and may improve the optical rear reflectance and/or the contact properties. In general, the efficiency potential of solar cells with carrier-selective passivation layers is much higher compared to conventionally diffused c-Si cells, because recombination at the metal/c-Si contact is more effectively suppressed. In this review, we put some special emphasis on doped polycrystalline silicon (poly-Si) layers on a thin silicon oxide, which are according to our assessment the most promising carrier-selective layers for future industrial solar cells. In addition, we discuss a couple of other materials that attracted greater attention in silicon photovoltaics only recently and are already well known from organic photovoltaics as carrier-selective layers. These materials include metal oxides, such as molybdenum oxide and titanium oxide, as well as conducting polymers. Finally, we compare the various options for carrier-selective passivation layers in terms of their selectivities and their efficiency potential.

2. Present status of surface passivation in industrial solar cells

In this review, we do not intend to provide a complete historic overview of the evolution of the various surface passivation schemes. For such an overview, the reader is referred to the existing comprehensive review papers [1,2]. We rather focus here on the major passivation schemes applied in today's industrial c-Si solar cells. The large majority of today's industrial cells feature high-temperature-diffused emitters and/or back surface fields. Section 2.1 will hence focus on the passivation of such dopant-diffused silicon surfaces. The passivation of undiffused silicon surfaces will then be discussed in Section 2.2. As the metal/c-Si interface recombination of today's industrial solar cells contributes quite significantly to the overall recombination losses, we also briefly discuss these regions in Section 2.3.

2.1. Passivation of dopant-diffused silicon surfaces

2.1.1. Phosphorus-diffused silicon surfaces

Fig. 3 schematically shows the band diagram of a PERC-type cell in the non-contacted region along the line A-B in Fig. 1. We start our discussion with the front passivation of the electron-selective phosphorus-diffused n^+ emitter. The overall recombination activity of the emitter is described via its recombination current density parameter J_0 (given in fA/cm^2), which is also often referred to as 'saturation current density' in the literature. J_0 includes both, the recombination within the bulk of the electron-selective n^+ emitter as well as at its surface. Another very important parameter is the sheet resistance of the n^+ emitter, characterizing the lateral conductivity for the electrons. Any material that is on the path of the electrons from the point of generation to the metal contacts contributes to recombination and to the series resistance and will thus contribute to a small or large extend to limiting the cell efficiency.

It has been known for decades that phosphorus-diffused n^+ emitters are very effectively passivated by means of silicon dioxide (SiO_2) grown at high temperature (typically > 900 °C) [3–5]. SiO_2 was hence used as standard surface passivation scheme in the early high-efficiency laboratory-type silicon solar cells developed in the 1980s and 90 s [6–8]. However, the high-temperature oxidation turned out to be less suitable for industrial solar cells because of several practical issues, such as too high production cost and the sensitivity of the silicon bulk material properties to high temperatures. Hence, an alternative low-temperature passivation scheme, plasma-enhanced chemical-vapor-deposited (PECVD) silicon nitride (SiN_x), which was routinely applied in microelectronics then, was in the 1980s transferred to photovoltaics [9,10]. In the 1990s, numerous studies analyzed and optimized the surface passivation properties of SiN_x layers on undiffused and diffused silicon surfaces [11–14] and it turned out that an unexpectedly high level of

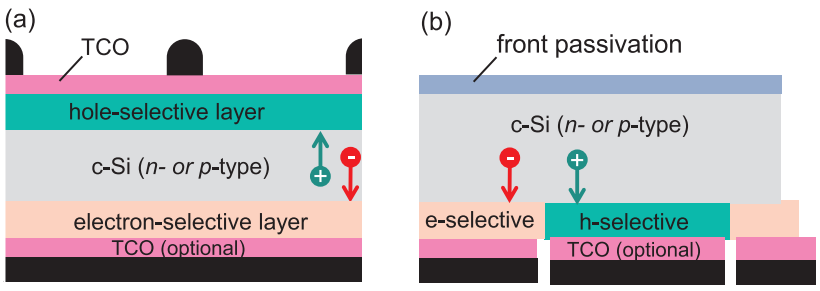

Fig. 2. Schematics of a (a) both-sides-contacted and (b) rear-side-contacted c-Si solar cell featuring hole- and electron-selective passivation layers. The transparent conductive oxide (TCO) at the cell rear can improve the rear reflectance and is optional, whereas the front TCO in the case of the both-sides-contacted cell shown in (a) is required to provide the lateral carrier transport to the front grid fingers.

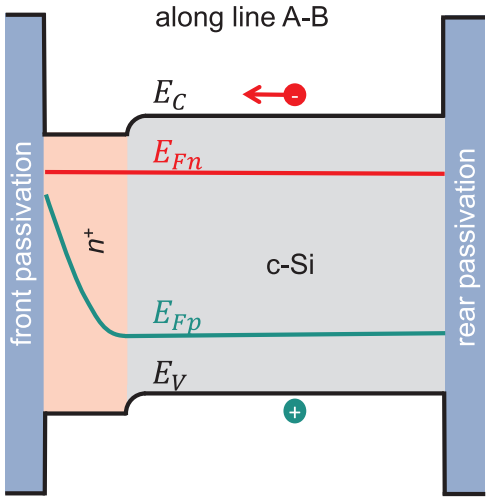

Fig. 3. Idealized band diagram in the dielectrically passivated region of the c-Si solar cell along line A-B denoted in Fig. 1.

surface passivation can be achieved, even after high-temperature firing as used for the contact formation of screen-printed metal contacts in industrial solar cells [15,16]. In addition, the refractive index of SiN_x films can be easily tuned by adjusting the film composition and the SiN_x films are hence also suited as excellent antireflection coatings when applied to the front of silicon solar cells. All these factors together made SiN_x films the standard front coating in today's P-diffused industrial silicon solar cells.

Fig. 4 shows an exemplary set of measured recombination current density parameters J_0 on planar PECVD-SiN_x-passivated n^+ emitters as a function of the sheet resistance in comparison with two high-temperature SiO_2-based passivation schemes [17]. In order to realize the best-case passivation scenario as a reference, the single-layer SiO_2-passivated samples included in Fig. 4 received a so-called 'alneal', which consists of the deposition of a thin Aluminum layer on top of the SiO_2, an annealing step at ~ 400 °C and a subsequent removal of the Aluminum. This procedure generates atomic hydrogen by a reaction between residual water molecules within the SiO_2 layer and the Aluminum [18]. The atomic hydrogen is then able to effectively passivate dangling bonds at the c-Si/SiO_2 interface, thereby drastically reducing the interface state density and consequently improving the passivation quality. The alnealed thermally grown SiO_2 is regarded as the best-case reference scenario. In addition to the single-layer SiO_2 and SiN_x passivation layers, a stack consisting of a thin (~ 10 nm) thermally grown SiO_2 plus a thicker (~ 60 nm) PECVD-SiN_x capping layer is included in

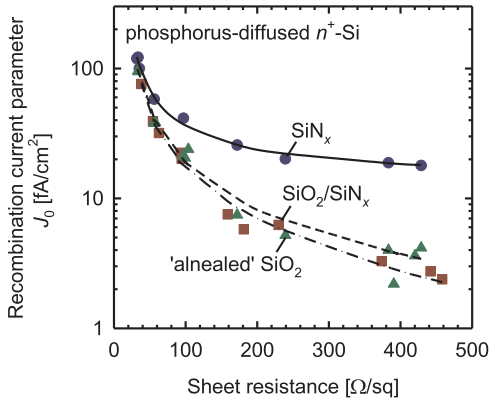

Fig. 4. Measured recombination current density parameter J_0 as a function of the sheet resistance for planar phosphorus-diffused n^+ emitters passivated by (i) 'alnealed' thermally grown SiO_2, (ii) PECVD-SiN_x, and (iii) SiO_2/SiN_x stacks [data taken from Ref. [17]].

Fig. 4 as well. It is obvious that the SiO_2/SiN_x stack provides as effective a surface passivation as the alnealed SiO_2 reference, although it has a higher potential concerning the transfer to an industrial cell process. This improved passivation behavior of the SiO_2/SiN_x stack has been attributed to the very high hydrogen content in the PECVD-SiN_x layer (> 10 at%) [17]. The atomic hydrogen diffuses through the thin SiO_2 layer and passivates dangling bonds as effective as in the case of the annealing treatment. Typical sheet resistances of industrial n^+ emitters are in the range between 80 and 140 Ω/sq. In this most relevant range, the emitter with thermally grown SiO_2 and SiO_2/SiN_x stacks shown in Fig. 4 achieve J_0 values of 12–25 fA/cm^2 while the emitter with a single-layer SiN_x exhibits J_0 values of 30–40 fA/cm^2. Hence, SiN_x-passivated n^+ emitters show a high potential, which is, however, outperformed by SiO_2/SiN_x stacks, which perform as excellently as the alnealed SiO_2 reference. Single layers of PECVD-SiN_x are the standard in the n^+ emitter passivation in today's industrial solar cells, however, as other recombination channels, such as bulk and rear surface recombination, are more and more reduced, the front emitter is becoming one of the performance-limiting factors in the next generation of industrial solar cells. Hence, the introduction of SiO_2/SiN_x stacks is an industrially feasible path to further enhance the potential of the n^+ front emitter, in particular in solar cells with selective emitters.

In order to reduce the front reflection and to improve light trapping, the solar cell front is textured, e.g. by random pyramids in the case of monocrystalline silicon solar cells, and the emitter is diffused into the textured surface. The effect of texturing on the surface passivation properties of SiO_2, SiN_x, and SiO_2/SiN_x stacks has been studied [19,20] and it was found that for typical industrial emitters, J_0 increases approximately by the fraction of the surface area increase, i.e. for random pyramids J_0 increases by a factor of 1.73. This leads for the best random-pyramid-textured state-of-the-art industrial selective emitters with a sheet resistance of ~ 120 Ω/sq in the shallow-diffused n^+ region to J_0 values of ~ 25 fA/cm^2, which have most recently indeed been realized on state-of-the-art > 22% efficient industrial PERC devices [21].

2.1.2. Boron-diffused silicon surfaces

The surface passivation of boron-diffused p^+ emitters, as required for the fabrication of high-efficiency *n*-type silicon solar cells, has been very challenging in the past. In some studies [22–24], it was shown that high-temperature-grown SiO_2 can initially passivate boron-doped p^+ emitters to a good level, however, other researchers [25] reported only a mediocre level of passivation. One of the biggest issues, however, was that under storage in atmosphere the passivation of boron-diffused p^+ emitters by thermally grown SiO_2 was found to be unstable even for the best initial passivation [24,26]. For sheet resistances of ~ 100 Ω/sq, low initial J_0 values of 30 fA/cm^2 have been measured on p^+ emitters passivated with SiO_2. After 2 years of storage in the drawer, however, the J_0 increased to ~ 300 fA/cm^2 [26]. The fact that high-temperature SiO_2-passivated boron-diffused p^+ emitters are unstable has also been observed on high-efficiency *n*-type 'passivated emitter and rear locally diffused' (PERL) silicon solar cells with p^+ front emitter, where a V_{oc} degradation by up to 100 mV was reported [24]. It was conjectured [27] that this instability is a result of the permeability of SiO_2 to moisture and that adding an effective moisture barrier, such as SiN_x, might reduce the degradation. In practice, however, there have been contradictory results published concerning the improved stability of p^+ emitters passivated by SiO_2/SiN_x stacks [24,25,27].

The standard passivation scheme of the phosphorus-diffused n^+ emitter in industrial *p*-type silicon solar cells is PECVD-SiN_x. Unfortunately, in the case of the boron-diffused p^+ emitter, as-deposited SiN_x turned out to be less favorable [23] and high J_0 values up to 1000 fA/cm^2 were measured for p^+ emitters passivated with PECVD-SiN_x [23]. In the literature, the poorer passivation quality of SiN_x on p^+ emitters compared to n^+ emitters had been attributed to the high positive fixed charge density within the SiN_x layer as well as to a highly

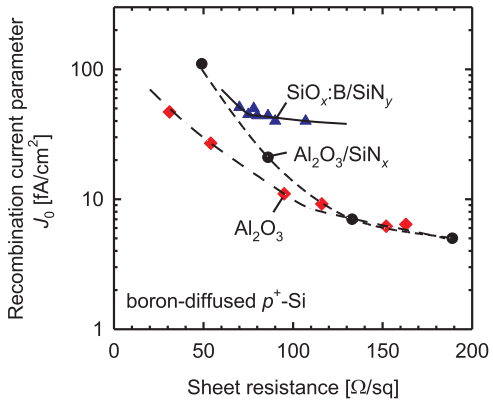

Fig. 5. Measured recombination current density parameters J_0 as a function of sheet resistance for boron-diffused p^+ emitters passivated by (i) atomic-layer-deposited Al_2O_3[29], (ii) Al_2O_3/SiN_x stacks [30], and (iii) stacks of boron silicate glass (SiO_x:B), simultaneously used as boron diffusion source, and an SiN_y capping layer [38].

asymmetric electron-to-hole capture cross section ratio of the interface states [26].

While the surface passivation of undiffused c-Si surfaces with aluminum oxide (Al_2O_3) has been investigated since the 1980s [10,28], it was only in recent years that boron-diffused p^+ silicon surfaces were successfully passivated. The best passivation results of boron-diffused p^+ emitters have been achieved by layers of plasma-assisted atomic-layer-deposited (ALD) Al_2O_3 [29]. The diamonds in Fig. 5 show results published in Ref. [29]. At a sheet resistance of 100 Ω/sq, a J_0 value of only 10 fA/cm^2 is achieved. Comparable results have been reported for Al_2O_3/SiN_x stacks [30] with an improved firing stability compared to single layers of Al_2O_3, as will be discussed in more detail in the next Section. The excellent passivation property of Al_2O_3 has mainly been attributed to the high negative fixed charge density in the Al_2O_3 layers. Importantly, the Al_2O_3-passivated p^+ emitters have proven to be perfectly stable under prolonged UV illumination [31] in contrast to SiN_x or SiO_2 passivation layers on n^+ emitters. More industrially suitable deposition techniques, such as PECVD and spatial ALD, have been successfully applied for the deposition of Al_2O_3 [32,33] and have been implemented into industrial *n*-type silicon solar cells.

Concerning the development of industrial *n*-type silicon solar cells with screen-printed metal contacts, today, the most frequently implemented structure is the 'passivated emitter and rear totally diffused' (PERT) cell architecture with an Al_2O_3/SiN_x-passivated homogeneous p^+ hole-selective emitter at the cell rear, today exceeding efficiencies above 21% [34,35]. This cell type has the additional charm that the process is very close to the dominant industrial PERC process flow. It comes even closer to the PERC process if the Al_2O_3/SiN_x passivation is omitted and instead a boron-containing oxide or oxynitride layer, sometimes denoted 'boron silicate glass' (BSG), is deposited at the cell rear using PECVD. Ideally, this BSG layer acts both as boron source for the p^+ emitter in-diffusion and as passivation layer [36]. The corresponding *n*-PERT cell process contains the same number of process steps as the standard *p*-PERC process [37], making it most attractive for industrial application. Fig. 5 shows measured J_0 values of such SiO_x:B/SiN_y-passivated p^+ emitters, demonstrating that although the overall passivation quality is inferior to that of Al_2O_3 or Al_2O_3/SiN_x stacks, the BSG passivation still provides a sufficient level of surface passivation with J_0 values around 40 fA/cm^2 for sheet resistances of ~100 Ω/sq [38].

2.2. Passivation of undiffused surfaces

The right-handed surface in the band diagram shown in Fig. 3 is undiffused. It is characterized by its effective surface recombination velocity S_{eff} or, equivalently, by its corresponding recombination current density parameter $J_0 = qn_0S_{eff}$, with $n_0 = n_i^2/p_0$ being the equilibrium electron concentration, p_0 the equilibrium hole concentration (acceptor concentration) and n_i the intrinsic carrier concentration of the silicon *p*-type bulk. Note that in most dielectric passivation layers a charge density forms within the layer or at its interface with c-Si, inducing a band bending in the c-Si close to the surface. The resulting space charge region in the silicon towards the surface is not included in Fig. 3, because S_{eff} includes via definition recombination at the interface as well as within the space charge region. Hence, in Fig. 3, the edge of the corresponding space charge region is identified with the surface.

The passivation of the undiffused rear surface of solar cells made on *p*-type silicon wafers was one of the major technological improvements in the industrial solar cell production within the past decade, which led to industrial PERC cells with efficiencies exceeding 22% [21,39]. In the first attempts to implement an industrially suitable low-temperature rear passivation scheme, motivated by the excellent results obtained on lifetime samples [13,14], plasma-enhanced chemical vapor deposited SiN_x was evaluated in PERC-type lab solar cells [17,40]. Unfortunately, the short-circuit current densities of PERC devices with SiN_x rear surface passivation were severely reduced compared to reference solar cells with high-temperature SiO_2 rear surface passivation. It was shown [41] that this effect can be attributed to the high density of fixed positive charges within the SiN_x layer when deposited onto a c-Si surface, inducing an inversion layer in the crystalline silicon underneath the SiN_x. The coupling of this inversion layer to the base contact leads to a significant loss in the short-circuit current density, a detrimental effect named 'parasitic shunting' [41]. An effective method to prevent the parasitic shunting is to introduce a thermally grown, typically ~ 10 nm thick SiO_2 layer between the *p*-type silicon surface and the SiN_x layer, which was successfully demonstrated on laboratory-type PERC devices [17]. As the fixed positive charge density in SiO_2 on c-Si is considerably lower compared to SiN_x, parasitic shunting is absent on *p*-type silicon surfaces passivated with SiO_2/SiN_x stacks. Furthermore, it was demonstrated that the surface passivation by SiO_2/SiN_x stacks improves considerably during high-temperature annealing, which was attributed to the diffusion of hydrogen from the hydrogen-rich PECVD-SiN_x layer to the SiO_2/c-Si interface, where the hydrogen effectively passivates silicon dangling bonds [17].

In recent years, the negative-charge dielectric aluminum oxide (Al_2O_3) has proven capable of providing an outstanding level of passivation on crystalline silicon surfaces [10,42–50,56]. Al_2O_3 dielectric layers were first demonstrated by Jaeger and Hezel [10,28] in the 1980s to effectively passivate crystalline silicon surfaces. However, these first promising results were not taken up by the photovoltaic community then, until almost two decades later surface recombination velocities below 10 cm/s were demonstrated on *p*-type silicon wafers using atomic-layer-deposited Al_2O_3 [42,43]. This was the beginning of the 'revival' of Al_2O_3 as a dielectric passivation layer with striking properties, which later turned out to be perfectly suited for the application to the rear surface passivation of industrial PERC solar cells. Al_2O_3 can be deposited by various techniques, such as atomic layer deposition (ALD) leading to the best passivation properties [42,43], plasma-enhanced chemical vapor deposition (PECVD) [32,44,49,50], inductively coupled plasma (ICP) deposition [51], atmospheric pressure chemical vapor deposition (APCVD) [10,52], or reactive sputtering [45]. It was demonstrated to be ideally suited to the rear passivation of PERC solar cells, as the above-mentioned parasitic shunting is completely absent – thanks to the fixed *negative* charges [53].

As mentioned above, industrial-type solar cells use screen-printing of metal pastes and firing in a belt-line furnace at high temperatures (750–850 °C) for contact formation, which makes an excellent thermal stability of the surface passivation indispensable. Ultrathin ALD-Al_2O_3 layers tend to degrade during this firing step; however, a hydrogen-containing SiN_x capping layer deposited by PECVD improves the firing stability considerably [46]. Comparable results were obtained for

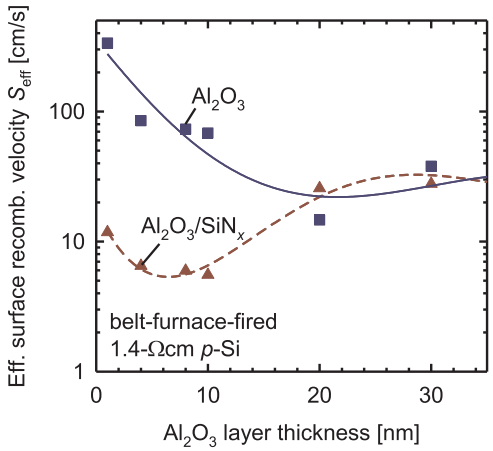

Fig. 6. Effective surface recombination velocity S_{eff} measured at a fixed excess carrier concentration of $\Delta n = 10^{15}$ cm^{-3} as a function of Al_2O_3 layer thickness after firing. Shown are the results for single Al_2O_3 layers and Al_2O_3 layers with SiN_x capping layer. The Al_2O_3 layers were deposited using plasma-assisted atomic-layer-deposition (ALD), whereas the SiN_x films were deposited using plasma-enhanced chemical vapor deposition (PECVD) [data taken from Veith et al., Ref.[55].

Al_2O_3/SiN_x layers deposited by ICP and PECVD [51] when optimizing the thermal budget of the SiN_x capping layer deposition [54] thereby reducing blistering of the passivation layer stack. Please note that the SiN_x capping layer also serves as a protection layer, since the Al_2O_3 is not stable against the aluminum paste used at the rear of PERC cells. Fig. 6 shows an exemplary result of measurements of the effective surface recombination velocity S_{eff} after firing for different layer systems as a function of Al_2O_3 layer thickness (taken from Ref. [55]. For ALD-Al_2O_3 single layers thinner than 20 nm a pronounced increase of S_{eff} after firing is observed, whereas Al_2O_3/SiN_x stacks with Al_2O_3 layers in the range between 4 and 10 nm exhibit S_{eff} values of around 6 cm/s after firing, which corresponds to a low J_0 of only 10 fA/cm^2 for an acceptor concentration of $N_A = 10^{16}$ cm^{-3}. Hence, Al_2O_3/SiN_x stacks are well suited for the application to the rear surface passivation of screen-printed PERC solar cells and were hence an important milestone on the path towards the industrialization of the PERC cell. Meanwhile, many solar cell manufacturers have introduced Al_2O_3/SiN_x stacks as rear passivation of industrial PERC solar cells into mass production.

2.3. Passivation of the contacts

Contacting a solar cell requires a metal/semiconductor interface that typically shows strong recombination. For this reason it is advantageous to cover only a few percent of the cells front and rear side area with a metal. As the surface recombination velocity of a metal-contacted silicon surface is extremely large ($> 10^5$ cm/s), a metal that covers only 1% of the surface of a 2 Ω cm c-Si wafer produces already an unacceptably large J_0 of around 2000 fA/cm^2. Metal contacts of high-efficiency cells do thus require an effective means of contact passivation.

Today's PERC-type solar cells use high doping underneath the metal contacts as a means of contact passivation. Fig. 7 shows a schematic of the band diagram and the quasi-Fermi levels in the contacted region of a PERC device. At the negative-metal contact an electron-selective n^+ emitter allows electrons to flow from the c-Si wafer through emitter to the contact. Fig. 7 shows an n^+ emitter with some recombination at the metal/n^+-emitter interface remaining. The overall recombination is, however, largely reduced compared to the case without the diffused n^+ emitter region. The recombination current density parameter $J_{0,e}$ includes recombination within the bulk of the n^+ emitter and at the metal/n^+ emitter interface.

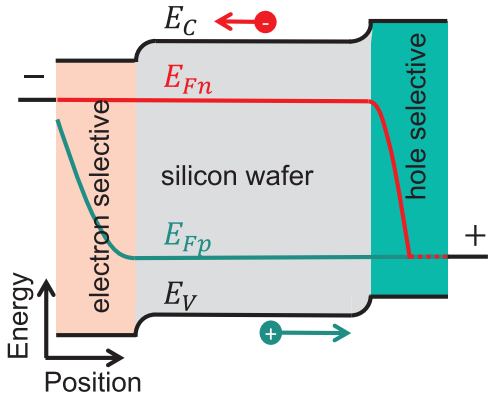

Fig. 7. Idealized band diagram in the contacted regions of a silicon solar cell. The diagram is taken along the line C-D in Fig. 1.

As an example, we chose a screen-printed PERC-type solar cell with an efficiency of 21.2%, which has been comprehensively characterized and can be considered as typical case for today's industrial PERC solar cells [56]. In this device, the n^+ emitter is characterized by a $J_{0,e}$ value of 109 fA/cm^2 and a contact resistance $\rho_{c,e}$ of 0.26 Ωcm^2 [57]. Please note that this resistance contains resistance contributions from the lateral current flow in the emitter and from the c-Si/metal interface. It is thus affected by the front contact grid spacing. We enter this data pair ($J_{0,e}$, $\rho_{c,e}$) into the first row of Table 1. Table 1 gives an overview over various types of electron-selective contacts reported in the literature and discussed throughout this review.

The low hole conductivity of the n^+ emitter region hinders the holes in reaching the recombination sites. This reduces $J_{0,e}$ and thus causes contact passivation. Note that locally increasing the doping underneath the metal contacts is capable of further reducing $J_{0,e}$ (a concept that is called 'selective emitter'), however, this comes at the cost of increased process complexity. Here, we only consider the case of a homogeneously diffused n^+ emitter. The other important parameter of the front contact is its contact resistance $\rho_{c,e}$ (in Ω cm^2). Please note that the effective recombination current density parameter in the solar cell is $f_e \times J_{0,e}$ rather than $J_{0,e}$ for a contacted area fraction f_e. The effective resistance of the device scales inversely with the area fraction and is $\rho_{c,e}/f_e$ rather than ρ_e. Thus, the effective device parameters are f_e $J_{0,e}$ and $\rho_{c,e}/f_e$. The metallization fraction f_e has therefore to be optimized for reaching an optimum efficiency η_{max} at the best compromise for low recombination losses and low resistive losses.

In the same way, a hole-selective region separates the positive contact from the c-Si wafer. In a PERC-type cell, the hole-selective

Table 1
Experimental recombination current density parameters $J_{0,e}$ and contact resistances $\rho_{c,e}$ of electron-selective contacts taken from the given references. The resulting selectivities $S_{10,e}$, the efficiency-maximizing contacting area fraction $f_{e,max}$ and the maximum efficiency $\eta_{e,max}$ are calculated using Eqs. (6), (8), (13), and (14).

Electron-selective	$J_{0,e}$ [fA/cm^2]	$\rho_{c,e}$ [Ω cm^2]	Ref.	$S_{10,e}$	$f_{e,max}$ [%]	$\eta_{e,max}$ [%]
P-diffused n^+	109	0.26	[57]	12.0	44.0	25.0
a-Si:H(i)/a-Si:H(n)	2	0.1	[58]	14.1	57.9	28.6
SiO_x/poly-Si(n^+) *[thermal oxide/PECVD]*	5	0.016	[84]	14.5	14.1	28.9
SiO_x/poly-Si(n^+) *[thermal oxide/LPCVD]*	2.7	0.0013	[59]	15.9	5.22	29.2
SiO_x/poly-Si(n^+) *[chemical oxide/LPCVD]*	10	0.0001	[60]	16.4	0.744	29.2
SiO_x/TiO_2	50	0.026	[133]	13.3	7.27	27.7
MgO_x	950	0.0175	[134]	12.2	3.06	25.5

Table 2
Experimental recombination current density parameters $J_{0,h}$ and contact resistances $\rho_{c,h}$ of hole-selective contacts taken from the given reference. The resulting selectivities $S_{10,h}$, the maximum efficiencies $\eta_{h,max}$ and the efficiency-maximizing contacting area $f_{h,max}$ are calculated from the measured data using Eqs. (6), (8), (13), and (14).

Hole selective	$J_{0,h}$ [fA/cm^2]	$\rho_{c,h}$ [Ω cm^2]	Ref.	$S_{10,h}$	$f_{h,max}$ [%]	$\eta_{h,max}$ [%]
Al-doped p^+	550	0.005	[61]	13.0	1.14	27.2
a-Si:H(i)/a-Si:H(p)	2	0.4	[58]	13.5	132	28.0
SiO_x/poly-Si(p^+) *[chemical oxide/PECVD]*	16	0.008	[85]	14.3	5.67	28.8
SiO_x/Si:C(p^+) *[chemical oxide/PECVD]*	11.5	0.017	[88]	14.1	9.95	28.6
a-Si:H(i)/MoO_x	10	0.4	[128]	12.8	8.41	26.9
MoO_x	300	0.03	[139]	12.5	5.57	26.1
PEDOT:PSS	80	0.1	[132]	12.5	18.8	26.2

region is a locally formed Al-doped p^+ back surface field (BSF) that forms during the firing process. Holes can easily pass and thus allow for a low contact resistance $\rho_{c,h}$, while electrons are blocked and thus cause a low recombination current density parameter $J_{0,h}$. Please note that Fig. 7 illustrates the special case of an electronically non-transparent p^+ region that cannot be fully passed by light-generated excess electrons generated in the absorber.

As an example, we consider the local screen-printed Al contacts of the above 21.2%-efficient PERC-type cell with experimentally extracted parameters of the Al-p^+ region of $J_{0,h} = 550\,\mathrm{fA/cm^2}$ and $\rho_{c,h} = 5\,\mathrm{m\Omega\,cm^2}$ [57,61]. We enter this data pair into the first row of Table 2. Table 2 lists various hole-selective contacts that are discussed throughout this review.

3. The concept of carrier selectivity

3.1. Definition of selectivity

The above discussion showed that carrier-selective layers should allow one polarity of charge carriers to pass to the metal and should block the other polarity. The carrier selectivity is thus related to the resistance that the selective layer has for majority carriers and minority carriers, respectively [62–64]. Let us assume that the carrier-selective contact has a total recombination rate $R(V)$ (in $\mathrm{cm^{-2}\,s^{-1}}$) that depends on the internal quasi-Fermi level splitting $V = (E_{Fn} - E_{Fp})/q$ at the contact. Then, the resistance for minority carriers (m) is

$$\rho_m = \frac{V}{q\,R(V)}, \tag{1}$$

where q is the elementary charge. The resistance for the majority carriers (M)

$$\rho_M = \rho_c \tag{2}$$

equals the contact resistance ρ_c at the point of operation. The ratio of the resistances thus is

$$\frac{\rho_m}{\rho_M} = \frac{V}{q\,R(V)\,\rho_c} = \frac{V_{th}}{\rho_c\left(\frac{qR(V)}{e^{\frac{V}{V_{th}}}-1}\right)} \quad \frac{V}{V_{th}\left(e^{\frac{V}{V_{th}}}-1\right)} = S(V)\;\; g(V) \tag{3}$$

and can be written as the product of what was defined to be the selectivity of the contact [63]

$$S(V) = \frac{V_{th}}{\rho_c\left(\frac{qR(V)}{e^{\frac{V}{V_{th}}}-1}\right)} \tag{4}$$

and a voltage-dependent factor

$$g(V) = \frac{V}{V_{th}\left(e^{\frac{V}{V_{th}}}-1\right)}. \tag{5}$$

Here, V_{th} is the thermal voltage and ρ_c is the contact resistance. The numerical values for S span many orders of magnitude. We therefore also define the logarithmically scaled selectivity

$$S_{10}(V) = \log_{10}(S(V)). \tag{6}$$

In general, S_{10} will depend on the operating point. Selecting the maximum power point leads to a selectivity value that is relevant for the ultimate device performance. In many important cases the recombination rate of the contact

$$R(V) = \frac{J_0}{q}\left(e^{\frac{V}{V_{th}}}-1\right) \tag{7}$$

follows the ideal Shockley diode equation. A highly doped surface region is such an important example. The ideality factor is unity even if Auger recombination dominates because a highly doped surface region stays in low injection. The contact resistance ρ_c is often voltage-independent. In these well behaved cases we find

$$S = \frac{V_{th}}{\rho_c J_0} \tag{8}$$

and the selectivities S and S_{10} become voltage-independent. J_0 is the recombination current density parameter. This voltage-independence of S and S_{10} for well-behaved contacts is a consequence of factoring out $g(V)$ from the resistance ratio in Eq. (3) when defining S. The advantage of a selectivity that is independent of the point of operation is, that it allows a direct comparison of the selectivities of different contact schemes with a single number. We do not have to know the maximum power point that will always depend on many other properties than just the type of selective contact. For not well-behaved contacts the general definition given by Eq. (4) has to be applied at a reference point, e.g. the maximum power point of the cell.

To illustrate the concept of the selectivity S, let us consider a well-defined example, such as an Al-doped p^+ back surface field region. The recombination of this contact is quantified by an electron diffusion length L_n within the p^+ region and a recombination velocity S_n at the Al/p^+-Si interface. The well-known recombination current parameter of this contact is then given by the equation

$$J_{0,c} = q\frac{n_0 D_n}{L_n}\,\frac{\sinh\left(\frac{W_{p+}}{L_n}\right) + \frac{S_n L_n}{D_n}\cosh\left(\frac{W_{p+}}{L_n}\right)}{\cosh\left(\frac{W_{p+}}{L_n}\right) + \frac{S_n L_n}{D_n}\sinh\left(\frac{W_{p+}}{L_n}\right)}, \tag{9}$$

where n_0 is the equilibrium minority-carrier concentration within the Al-p^+ region, D_n is the electron diffusivity and W_{p+} is the width of the Al-p^+ region. Since the contact resistance

$$\rho_c = \frac{1}{q\,p_0\,\mu_p}\,W_{p+} \tag{10}$$

is inversely proportional to the equilibrium majority carrier concentration p_0, the selectivity S as given by Eq. (8) is proportional to p_0/n_0. In Eq. (10), μ_p denotes the hole mobility within the Al-p^+ region.

The detailed calculation [64] shows that

$$S = \frac{p_0\ \mu_p}{n_0\ \mu_n} \propto \frac{p_0}{n_0} \tag{11}$$

for the electronically transparent case where the recombination at the c-Si/metal interface is strong and is thus limited by transport towards the interface. Depending on the doping (or the band bending in other structures), the ratio p_0/n_0 easily spans 18 orders of magnitude and always controls the selectivity as the mobilities μ_n for electrons and μ_p for holes are of the same order of magnitude in c-Si [64]. It becomes immediately evident from Eq. (11) that increasing the doping underneath the metal contact, i.e. increasing p_0 and hence decreasing n_0, directly increases the selectivity.

3.2. Properties of the selectivity

The selectivity has the following general properties [63,64] as a consequence of the above definition:

(1) The selectivity is a property of the selective contact only. It is in general dependent on the point of operation (i.e. the internal quasi-Fermi level splitting) and independent of other properties of a solar cell.
(2) The selectivity S is proportional to the ratio of resistances that the selective contact has for majority and minority carriers, respectively. The factor of proportionality $g(V)$ is chosen to remove the voltage dependence from S for the well-behaved cases of constant contact resistance for majority carriers and recombination characteristics following the Shockley diode equation.
(3) If the selectivity S of a first selective contact is larger than that of a second selective contact, then a cell with the first contact will allow a higher efficiency than a cell with the second contact if the areal fraction of this contact is optimized and if all other properties of the cell are assumed to be ideal.
(4) The efficiency potential of an ideal c-Si solar cell with a single selective contact of selectivity S_{10} increases linearly with S_{10} until finally the limitation by the intrinsic lifetime of c-Si sets in.

It is the last property that makes the logarithmic selectivity S_{10} a valuable figure of merit that allows comparing the ultimate efficiency potential of various types of selective layers. Assuming a c-Si wafer thickness of 110 µm, Lambertian light trapping and only intrinsic recombination, the limiting efficiency for a 2-Ω cm n-type silicon wafer is

$$\eta_{max} = (2.452\ \ S_{10} - 4.240)\ \ \% \tag{12}$$

in the case where the overall recombination is not limited by the intrinsic bulk recombination and is

$$\eta_{max} = ((2.452\ \ S_{10} - 4.240)^{-19.52} + (29.21)^{-19.52})^{-\frac{1}{19.52}}\ \ \% \tag{13}$$

otherwise [63]. Fig. 8 shows this function that is linear in selectivity for $S_{10} < 13$ as described by Eq. (12) and is increasingly limited by intrinsic recombination in the ideal c-Si wafer for $S_{10} > 13$ as described by Eq. (13). For selectivity values $S_{10} > 16$, the cell does no longer "see" the contact and the reduction of the cell performance due to the selective contact is negligible relative to recombination and resistance losses of the c-Si wafer.

If the efficiency of a solar cell with a contact of selectivity S is limited by recombination (large J_0) rather than by resistance (large ρ_c), it is advantageous to reduce the contact area f to a value

$$f_{max} = \rho_c/\rho_{max}(S_{10}) \tag{14}$$

that maximizes the cell efficiency. For the above defined ideal cell with a single non-ideal selective contact of selectivity S_{10} the function ρ_{max} is [63]

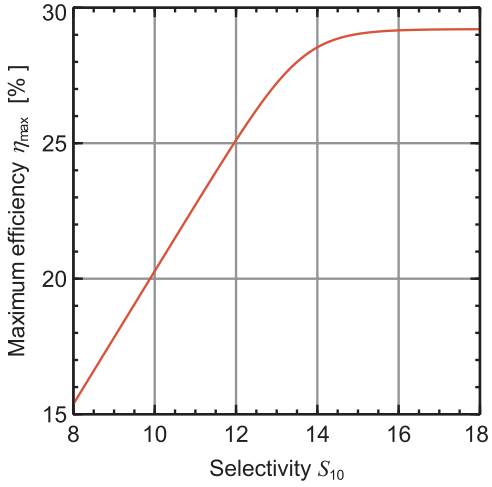

Fig. 8. Maximum efficiency $\eta_{max}(S_{10})$ according to Eq. (13) assuming a 2 Ω cm n-type c-Si wafer of thickness W = 110 µm with Lambertian light trapping (J_{sc} = 43.6 mA/cm^2) and intrinsic bulk recombination with a single contact of selectivity S_{10}. The second contact is assumed to be ideal.

$$\rho_{max} = \left(0.6271^{\ -1.805} + \left(1.620 \times 10^6\ \ e^{-\frac{S_{10}}{0.8819}}\right)^{-1.805}\right)^{-\frac{1}{1.805}} \Omega cm^2. \tag{15}$$

3.3. Ideal solar cell with two non-ideal selective contacts

If an otherwise ideal cell has an electron-selective contact of selectivity

$$S_{10,e} = \log_{10}\left(\frac{V_{th}}{J_{0,e}\ \rho_{c,e}}\right) \tag{16}$$

and a hole-selective contact of selectivity

$$S_{10,h} = \log_{10}\left(\frac{V_{th}}{J_{0,h}\ \rho_{c,h}}\right), \tag{17}$$

it is possible to prove that the maximum achievable combined selectivity $S_{e\&h,\ max}$ that determines the maximum achievable efficiency of this cell via Eq. (13) is given by [64]

$$S_{e\&h,\ max} = \frac{1}{\left(\frac{1}{\sqrt{S_e}} + \frac{1}{\sqrt{S_h}}\right)^2}. \tag{18}$$

Here, S_e and S_h are both defined by Eq. (8) when applied to electron- and hole-selective contacts, respectively. A cell with two contacts has the effective device parameters ($\rho_{c,e}/f_{e,max} + \rho_{c,h}/f_{h,max}$) and ($f_{e,max}\ J_{0,e} + f_{h,max}\ J_{0,h}$). Contact fractions $f_{e,max}$ and $f_{h,max}$ that maximize the efficiency are

$$f_{e,\ max} = \frac{\rho_{c,e} + \sqrt{\frac{\rho_{c,h} J_{0,h}\ \rho_{c,e}}{J_{0,e}}}}{\rho_{max}(S_{10,e\&h,\ max})} \tag{19}$$

and

$$f_{h,\ max} = \frac{\rho_{c,h} + \sqrt{\frac{\rho_{c,e} J_{0,e}\ \rho_{c,h}}{J_{0,h}}}}{\rho_{max}(S_{10,e\&h,\ max})} \tag{20}$$

using Eq. (15) to determine $\rho_{max}(S_{10,e\&h,\ max})$.

4. Future surface passivation concepts

4.1. Poly-Si layers on oxide

Excellent carrier-selective contacts based on hydrogenated amorphous silicon (a-Si:H) layers are well known and have recently led to the current record efficiency for c-Si solar cells of 26.7% [65,66]. This type of carrier-selective contact, also known as HIT ('heterojunction with intrinsic thin layer') contact [137], is based on a thin intrinsic a-Si:H(i) layer plus a thicker doped a-Si:H(p or n) layer on top. In this review, we do not include a detailed discussion of the current state of HIT-type contacts based on amorphous silicon, but include typical J_0 and ρ_c data in Tables 1, 2 and 4 for comparison. For more detailed information, the interested reader is referred to a recently published review paper [67]. We rather focus here on passivating contacts based on stacks of an interfacial ultrathin Si oxide (SiO_x) covered by a heavily doped and (partially) crystallized silicon layer (the so called 'poly-Si' layer), a concept which has been investigated in bipolar microelectronics and photovoltaics [68–74] and has a large potential of being integrated into today's industrial solar cell production.

Regarding preparation of the latter stack, the interfacial SiO_x layer can either be grown thermally [75,76], wet-chemically [77–81] or in a dry ozone atmosphere [77,80]. The silicon layers can be deposited on top of the interfacial oxide by various techniques, such as low-pressure chemical vapor deposition (LPCVD) [76,80-83] or plasma-enhanced chemical vapor deposition (PECVD) [79,80,83-88]. Eventually, the junction is formed during annealing at high temperatures in the range of 800–1050 °C. The optimum annealing temperature depends on the interfacial oxide stoichiometry and thickness, the doping density within the silicon layer, and other process-related aspects.

Regarding the notation, "poly-Si emitters" or "semi-insulating poly-Si (SIPOS) emitters" [75,90] were used in the first reports of this contact scheme. After its recent revival [79,91-93], different renominations have been proposed. The most prominent one is "Tunnel oxide passivating Contact" (TopCon), which originally refers to a stack of an interfacial oxide and a Si-rich layer with a further component which increases the band gap and prevents a full crystallization during an anneal at 800–900 °C [79]. While this research group did not disclose the additional component explicitly, other groups recently reported on Si:C layers [88]. As there is theoretical [94–96] and experimental [88,97-100] evidence that homogenous tunneling through the interfacial oxide is not the only current transport mechanism in these types of junctions, "POLy-crystalline Si on Oxide" (POLO) was proposed as a more general notation [93]. For Si layers with a certain oxygen content, nc-SiO_x instead of SIPOS was proposed as another denotation [89]. Regardless of its exact modification, for the sake of simplicity we will use the notation "poly-crystalline silicon" (poly-Si) in the following.

Due to the large number of recent publications on this topic, it is hardly possible to summarize the results of all research groups. Table 3 therefore lists some representative passivation properties reported for various types on n^+ and p^+ poly-Si junctions in terms of reported J_0 values on planar and random-pyramid-textured c-Si surfaces for three different types of interfacial oxides. Except for p^+ poly-Si junctions on textured c-Si surfaces, an exceptional passivation quality is obtained independent of the growth method of the interfacial SiO_x. Note that besides the excellent J_0 values also very low ρ_c values are obtained for the poly-Si contacts, making this contact system an ideal candidate for high-efficiency silicon solar cells. Table 3 contains some representative (J_0, ρ_c) pairs achieved using n^+ and p^+ poly-Si contacts. In order to explain the very low measured J_0 values, the reduction of the minority carrier density at the c-Si/SiO_x interface by an in-diffusion of dopants from the doped poly-Si layer into the c-Si substrate is not sufficient. This can be concluded from the fact that for doped polycrystalline silicon placed directly (i.e., without interfacial oxide) on the c-Si surface, high J_0 values are measured (e.g. > 500 fA/cm^2 in Ref. [94], or even 1138 fA/cm^2 in Ref. [87]). This compares to 1 fA/cm^2 in the case with interfacial oxide [94], although the in-diffused region is present in both cases. Therefore, the passivation of poly-Si junctions relies on a low recombination velocity at the interface between the c-Si surface and the interfacial silicon oxide [77]. Indeed, the surface recombination velocities S_{n0} and S_{p0} at the c-Si/SiO_x interface, as deduced from the measured J_0 values of n^+ and p^+ poly-Si junctions [94], are in excellent agreement with the results obtained for high-temperature-grown SiO_2 on boron- [26] and phosphorus- [101] doped c-Si surfaces with comparable surface doping concentrations. This is in particular remarkable since the oxide passivation in Refs. [100,101] was grown at much higher temperatures (1035 °C in Ref. [101]) than the thin interfacial oxides of the poly-Si junctions (grown at 600 °C in Ref. [94]). Due to this difference in oxidation temperature, one would expect a higher c-Si/SiO_x interface state density [102] for the interfacial oxide, at least in the as-grown state. However, the high-temperature step for the poly-Si junction formation after deposition of the doped silicon-rich layer possibly leads to a re-arrangement of the atomic bonds at the c-Si/SiO_x interface, resulting in a low interface state density as an energetically favorable state of the system.

It is well known that the c-Si/SiO_x interface state density can be reduced by introducing atomic hydrogen [103]. This measure has been shown to also improve the passivation quality of poly-Si junctions. Atomic hydrogen can be effectively introduced into poly-Si junctions by depositing a hydrogen-rich layer such as SiN_x [82] or Al_2O_3 [86,104] on top of the poly-Si layer, followed by either a post-deposition anneal at ~ 400 °C or by a fast-firing step at 800–900 °C [83]. An alternative method to introduce atomic hydrogen is the exposure to a hydrogen plasma at ~ 400 °C. The improvement of the poly-Si junction passivation quality upon atomic hydrogen supply is larger than that achievable by a forming gas anneal with molecular hydrogen. In our experience, the latter process only yields a negligible improvement as compared to the as-processed state (e.g. ~ 1%$_{rel}$ for the implied open circuit voltage). Depending on the poly-Si junction passivation quality after junction formation, the magnitude of improvement due to hydrogen supply is quite different. Junctions with an already excellent passivation quality (i.e., with an already low c-Si/SiO_x interface state density) after junction formation tend to improve less than junctions with a moderate passivation quality after high-temperature processing. In particular, poly-Si junctions based on very thin, presumably non-stoichiometric interfacial oxides, which can only be processed at temperatures of 850 °C and below, show a significant improvement upon hydrogen supply. In contrast, poly-Si junctions based on thicker interfacial oxides with optimum annealing temperatures above 900 °C [105] exhibit excellent passivation quality directly after junction formation. This indicates a different c-Si/SiO_x interface state density for the two cases after junction formation. As the passivation of dangling bonds at the interface with hydrogen might be unstable in the long term, it seems desirable to achieve a low c-Si/SiO_x interface state density based on Si–O bonds directly after junction formation. However, further research is required to evaluate the long-term stability of poly-Si junctions as a function of the degree of hydrogenation applied.

The importance of the c-Si/SiO_x interface state density for the passivation quality of SiRLO junctions is also reflected in the difference in J_0 for poly-Si junctions on (100)- and (111)-oriented c-Si surfaces. The latter is relevant for alkaline-textured c-Si surfaces. It has been shown that for n^+ (p^+) poly-Si junctions, the J_0 value on planar (111)-oriented c-Si surfaces is increased by about one order of magnitude as compared to the J_0 value on planar (100)-oriented surfaces [106], which is comparable to the difference of the c-Si/SiO_2 interface state densities [107,108]. The J_0 values of poly-Si junctions on planar (111)-oriented c-Si surfaces agree well with the values obtained on alkaline-textured (100)-oriented c-Si wafers [106]. Furthermore, it has been shown that the recombination at the c-Si/SiO_x interface is indeed dominating the J_0 of poly-Si junctions [77,109]. Auger recombination in the region in which dopants have diffused from the doped poly-Si layer into the c-Si substrate upon annealing plays a minor role [76,109].

Table 3
Selection of experimentally reported recombination current densities J_0 for differently doped poly-Si layers on ultrathin SiO_x prepared by different methods.

Poly-Si layer, doping	Interfacial SiO_x	c-Si surface	Post-dep. anneal	J_0 [fA/cm^2]	Ref.
PECVD poly-Si, intrinsic	thermal	planar	SiN_x, Al_2O_3 or H-plasma	14	[114]
PECVD poly-Si, n^+	thermal	planar	FGA	4.3	[84]
LPCVD poly-Si, n^+	thermal	planar	FGA	0.7	[115]
LPCVD poly-Si, n^+	thermal	planar	FGA	3.4	[82]
LPCVD poly-Si, n^+	ozone	planar	FGA	0.5	[80]
PECVD poly-Si, n^+	wet-chemical	planar	FGA	5	[84]
PECVD poly-Si, n^+	wet-chemical	planar	FGA	5.7	[87]
PECVD nc-SiO_x, n^+	wet-chemical	planar	FGA	8.8	[89]
LPCVD poly-Si, n^+	wet-chemical	planar	FGA	1.5	[80]
PECVD poly-Si, n^+	thermal	planar	SiN_x, Al_2O_3 or H-plasma	0.4	[80]
PECVD poly-Si, n^+	thermal	planar	SiN_x, Al_2O_3 or H-plasma	1	[114]
LPCVD poly-Si, n^+	thermal	planar	SiN_x, Al_2O_3 or H-plasma	2.2	[82]
LPCVD poly-Si, n^+	ozone	planar	SiN_x, Al_2O_3 or H-plasma	0.6	[80]
PECVD, TopCon, n^+	wet-chemical	planar	SiN_x, Al_2O_3 or H-plasma	9	[92]
PECVD, TopCon, n^+	wet-chemical	planar	SiN_x, Al_2O_3 or H-plasma	7	[116]
LPCVD poly-Si, n^+	wet-chemical	planar	SiN_x, Al_2O_3 or H-plasma	0.6	[80]
LPCVD poly-Si, n^+	thermal	textured	FGA	11	[80]
LPCVD poly-Si, n^+	ozone	textured	FGA	13	[80]
LPCVD poly-Si, n^+	wet-chemical	textured	FGA	29	[80]
LPCVD poly-Si, n^+	thermal	textured	SiN_x, Al_2O_3 or H-plasma	3.8	[80]
LPCVD poly-Si, n^+	thermal	textured	SiN_x, Al_2O_3 or H-plasma	4.2	[82]
LPCVD poly-Si, n^+	ozone	textured	SiN_x, Al_2O_3 or H-plasma	4.4	[80]
LPCVD poly-Si, n^+	wet-chemical	textured	SiN_x, Al_2O_3 or H-plasma	2.4	[80]
LPCVD poly-Si, n^+	wet-chemical	textured	SiN_x, Al_2O_3 or H-plasma	4.3	[82]
LPCVD poly-Si, p^+	thermal	planar	FGA	4.4	[76]
LPCVD poly-Si, p^+	ozone	planar	FGA	11	[80]
PECVD poly-Si, p^+	wet-chemical	planar	FGA	16	[84]
LPCVD poly-Si, p^+	wet-chemical	planar	FGA	8	[117]
PECVD poly-Si(Ga), p^+	thermal	planar	SiN_x, Al_2O_3 or H-plasma	0.7	[118]
LPCVD poly-Si, p^+	thermal	planar	SiN_x, Al_2O_3 or H-plasma	1	[83]
LPCVD poly-Si, p^+	thermal	planar	SiN_x, Al_2O_3 or H-plasma	3.8	[80]
LPCVD poly-Si, p^+	ozone	planar	SiN_x, Al_2O_3 or H-plasma	5	[80]
PECVD Si: C, p^+	wet-chemical	planar	SiN_x, Al_2O_3 or H-plasma	11.5	[88]
LPCVD poly-Si, p^+	wet-chemical	planar	SiN_x, Al_2O_3 or H-plasma	5	[117]
LPCVD poly-Si, p^+	thermal	textured	FGA	54	[80]
LPCVD poly-Si, p^+	ozone	textured	FGA	112	[80]
LPCVD poly-Si, p^+	wet-chemical	textured	FGA	71	[80]
LPCVD poly-Si, p^+	thermal	textured	SiN_x, Al_2O_3 or H-plasma	27	[80]
LPCVD poly-Si, p^+	ozone	textured	SiN_x, Al_2O_3 or H-plasma	48	[80]
LPCVD poly-Si, p^+	wet-chemical	textured	SiN_x, Al_2O_3 or H-plasma	40	[80]

Besides the c-Si/SiO_x interface state density, the capture cross sections of the interface states are the second factor determining the surface recombination velocity. It is known that for the c-Si/SiO_x interface states, the capture cross section for electrons is larger than that for holes at an energetic position near the center of the Si band gap [110]. This could be one explanation for the slightly higher J_0 values typically measured on p^+ poly-Si junctions as compared to those measured on n^+ poly-Si junctions.

For an excellent surface passivation of poly-Si junctions, it is not only necessary to minimize recombination at the *c*-Si/SiO_x interface. Additionally, minority carriers have also to be prevented from reaching the defect-rich poly-Si layer where they would recombine on the time scale of picoseconds [111–113]. On the other hand, to maximize the selectivity, majority carriers should easily reach the poly-Si layer without resistive losses. Note that this selective blocking of one carrier type by the interfacial oxide cannot be explained consistently for both n^+ and p^+ poly-Si junctions within the framework of the tunneling model [70,94,95].

The probably most important conclusion from Table 3 is that different research groups are achieving similar passivation qualities with poly-Si junctions, independent of (i) the interfacial oxide growth method, (ii) the poly-Si deposition method, (iii) the doping method and (iv) additional components in the poly-Si layer, such as carbon. This is a strong indication for the robustness of the fabrication process.

4.2. Alternative materials for selective contacts

Metal oxides and conductive polymers have been applied in organic photovoltaics as carrier selective layers [119,120], but have not been considered for application to c-Si solar cells until only recently [121,122].

Fig. 9 compiles valence and conduction band edges of different such materials compared to silicon on an absolute energy scale. The materials are arranged in order of decreasing work function shown as dotted horizontal lines from left to right. Note that the material properties have been taken from literature [119,120,123] and that varying the stoichiometry strongly modifies the energetic structure. Fig. 9 gives hence only an estimate of what to expect. Note that the materials compiled in Fig. 9 are typically not deposited as a single layer on top of the c-Si surface. In order to improve the interface passivation, either layers of intrinsic hydrogenated amorphous silicon (a-Si:H(i)) or silicon oxide (SiO_x) layers are implemented in between the carrier-selective material and the crystalline silicon surface. Such additional interfacial passivation layers have to be ultrathin (i.e., in the nm range), in order to avoid the hindrance of the majority carrier transport across these layers. The transport across these layers occurs most likely by quantum-mechanical tunneling or hopping. The details of the majority-carrier transport might, however, be quite complex and are not well understood so far. In addition, the majority transport mechanism might vary for the different material systems. Generally speaking, the materials shown in Fig. 9 with large work function (left of dashed vertical line) are suitable as hole-selective contact materials. This was in fact

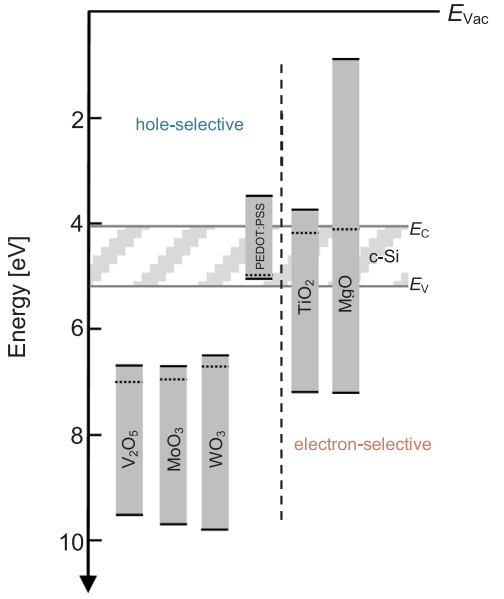

Fig. 9. Compilation of valence (lower solid lines) and conduction band edges (upper solid lines) together with their work functions (dotted lines) of different materials known from organic electronics [119,120,123], which are suitable as hole-selective contact materials (left of dashed vertical line) and electron-selective contact materials (right of dashed vertical line) on c-Si. For comparison the bandgap of crystalline silicon is also shown (cross-hatched rectangle).

experimentally confirmed on c-Si solar cells for the transition metal oxides vanadium oxide VO_x [124–126], molybdenum oxide MoO_x [126-129] and tungsten oxide WO_x [125,126,129] and also for the hole-conducting polymer poly(3,4-ethylene-dioxythiophene): polystyrenesulfonate (PEDOT: PSS) [121,130-132]. On the other side, the low-work-function materials TiO_x and MgO_x (right of dashed vertical line) have been demonstrated on c-Si solar cells to be suitable for the application to electron-selective contacts [133,134]. As the application of these materials to c-Si solar cells is a very young field of research, efficiencies achieved so far have not been able to keep up with the efficiencies obtained with poly-Si-based selective contacts. Despite the early state of the research, however, impressive efficiencies exceeding 22% have already been achieved with a-Si/MoO_x hole contacts [128] and SiO_x/TiO_2 electron contacts [133]. Also, very promising efficiencies exceeding 20% have been reported for PEDOT:PSS hole-selective layers [132] and for MgO_x electron-selective layers [134]. These four carrier-selective contact systems seem hence to be most promising and will therefore be discussed in more detail in the following. Nevertheless, there exist many more material systems, such as MgF_2 [135] or CsO_x [136], which might turn out to be more suitable for the application to c-Si solar cells. At the present point in time, however, due to the very early stage of the research, it is indistinct which material system might eventually be suitable for the implementation into next-generation commercial silicon solar cells. Hence, we focus here on the materials which already led to good cell efficiencies in the laboratory.

Considering the similarities in the electronic structures of the transition metal oxides VO_x, MoO_x and WO_x, we would expect a similar performance when applied to a c-Si solar cell. In fact, all three materials have been proven to be suitable as hole-selective contact materials on c-Si, with MoO_x resulting so far in the highest efficiency of 22.5% in combination with an intrinsic a-Si:H(i) interfacial passivation layer on an *n*-type silicon wafer [128]. Even if the metal oxides are non-stoichiometric, which is often the case when deposited as thin layers, the conductivity of the metal oxides is still relatively low, requiring very thin layers of only a few nm to be implemented into the cell contacts to allow for a good longitudinal hole transport. Hence, an additional well-conducting layer is required on top of the carrier-selective layer to provide the lateral majority-carrier transport to the metal contacts. This was in the case of the 22.5% efficient solar cells realized by a transparent conductive oxide (TCO) consisting of a bilayer of hydrogenated indium oxide and an indium tin oxide (ITO). Note that the work function of the TCO or the metal deposited on top of any carrier-selective layer can have a crucial impact concerning the functionality of the contact system and that a top layer with a mismatched work function can negatively impact the open-circuit voltage and the series resistance of the solar cell. In this review, we only consider conductive top layers that match the underlying carrier-selective materials. The cell architecture of the 22.5% efficient cell was based on the HIT ('heterojunction with intrinsic thin layer') cell concept [137] with only replacing the a-Si:H(*p*) layer by a 6 nm thick thermally evaporated MoO_x layer. The major benefit of this replacement is that due to the larger bandgap of MoO_x (~ 3 eV) compared to a-Si:H(*p*) (~ 1.7 eV), the optical losses are reduced, while maintaining the excellent passivation [128]. From the excellent V_{oc} of 725.4 mV of the 22.5% efficient cell, we estimate that the J_0 of the a-Si:H(i)/MoO_x/ITO hole-selective layer stack is in the order of 10 fA/cm^2. Due to the fact that replacing the a-Si (*p*) layer with the MoO_x resulted in practically the same *FF*s and efficiencies [128], we deduce that the contact resistance ρ_c is in the same order as that of the a-Si:H(i)/a-Si:H(*p*)/ITO stack, i.e. it is ~ 0.4 Ω cm^2 [138]. Omitting the a-Si:H(i) passivation layer leads to a significant increase in J_0 to ~ 300 fA/cm^2 and a decrease in ρ_c to ~ 30 mΩ cm^2 [139], which would suggest the application as local contacts in the latter case, as can also be seen from the calculated $f_{h,max}$ values in Table 2. Both cases are obviously very promising concerning their selectivity, which make transition metal oxides an interesting new material class for the application as hole-selective contacts in future c-Si solar cells.

Another very promising hole-selective material, which is routinely used in organic photovoltaics, but is new to silicon photovoltaics, is the hole-conducting polymer PEDOT:PSS [120]. In contrast to the above-discussed metal oxides, the conductivity of PEDOT:PSS layers can be very high up to ~ 1000 Ω^{-1}cm^{-1} and hence the transparent PEDOT:PSS layer does not need any TCO capping layer. Hence, the first c-Si solar cells with PEDOT:PSS were just based on depositing a PEDOT: PSS single-layer from the liquid solution onto the front of a silicon wafer, immediately achieving efficiencies > 10% [121,130,131]. Since, however, the parasitic absorption in PEDOT:PSS layers is still quite significant, these cells were limited with respect to their photocurrent. Higher efficiencies were obtained later by depositing the hole-collecting PEDOT:PSS to the cell rear and fully metallizing it with evaporated Ag. On the cell front, a conventional SiN_x-passivated phosphorus-diffused n^+ emitter was implemented. This so-called 'BackPEDOT' solar cell [140] led to a maximum efficiency of 20.6% [132] on a *p*-type silicon wafer. Concerning the quality of PEDOT:PSS as a hole-selective contact material on c-Si, the best J_0 values of around 50 fA/cm^2 were reported with an interfacial SiO_x layer, which came, however, at the cost of a very high contact resistance ρ_c > 1 Ω cm^2 [141], limiting the *FF* to values well below 80% and the efficiency to < 20%. In the 20.6% efficient cell, the SiO_x interfacial layer was omitted, still resulting in an acceptable J_0 of 80 fA/cm^2, but a drastically improved ρ_c of 0.1 Ω cm^2 [132]. The exact mechanism of surface passivation, in particular without SiO_x interfacial layer, is not known so far, but seems to be connected to the acidic nature of the PEDOT:PSS dispersion as well as the preferential energetic structure. Due to the hygroscopic nature of the PEDOT:PSS layer, instabilities in cell performance have been reported [131]. These instabilities, however, were shown to be completely avoidable after the PEDOT:PSS was capped by a metal foil impermeable to water [142]. Due to the simple deposition by spin- or spray-coating techniques from a liquid dispersion under ambient environment and the fact that PEDOT:PSS is a very cost-effective material, it is a promising low-cost candidate for contact passivation in future generations of c-Si solar cells. The parameters of some of the hole-selective contacts discussed are included in Table 2.

Less research has been devoted so far to alternative electron-selective contact materials. The most successful electron-selective material on c-Si so far, also well established in organic photovoltaics, is TiO_2. The highest efficiency of 22.1% was obtained for a stack of an ultrathin thermally grown tunnel-SiO_x (~ 1.2 nm) plus an atomic-layer-deposited 3.0 nm thick TiO_2 layer at the cell rear using *n*-type silicon base material [133]. Full-area rear metallization was performed by evaporating a few nm thin Al plus a thicker Ag layer. The cell front was conventionally processed by boron-diffusion of a p^+ hole-selective region, which was passivated using an Al_2O_3/SiN_x stack. It turned out that the TiO_2 layer thickness is essential concerning the contact properties. For the 22.1% efficient cell, a 3.0 nm thick TiO_2 layer resulted in a J_0 value of 50 fA/cm^2 and in a ρ_c of 26 mΩ cm^2 [133]. An only slight increase in the TiO_2 thickness to 3.5 nm resulted in an improvement of J_0 to 30 fA/cm^2, but also a pronounced increase in ρ_c to 60 mΩ cm^2 and in consequence to a decrease in efficiency to 21.6% [133]. Increasing the TiO_2 thickness in a SiO_x/TiO_2 stack further to 5 nm led to excellent J_0 values of 9 fA/cm^2 [143], however, at the cost of a very high ρ_c of 0.78 Ω cm^2, leading to a lower selectivity compared to the stack applied in the 22.1% cell. These results have been published within the last years only and demonstrate already the great potential of TiO_2-based electron-selective contacts. An even more recent development are MgO_x-based electron-selective contacts. Only very recently, a solar cell with an efficiency of 20.0% has been reported on *n*-type silicon with a thermally evaporated MgO_x/Al electron-selective contact at the cell rear [134]. As no interfacial SiO_x or a-Si:H(i) passivation was implemented in this contact, a relatively high J_0 of 950 fA/cm^2 was obtained, however, at an excellent ρ_c value of 17.5 mΩ cm^2 for the optimal MgO_x layer thickness of 1 nm. The main effect of placing a MgO_x layer in-between the *n*-Si wafer and the Al is hence to produce an ohmic contact with low ρ_c, avoiding the typical diode-like characteristic of the *n*-Si/Al junction. Reducing the contact area or implementing an interfacial passivation layer are possible measures to reduce recombination at the c-Si/MgO_x/Al contact. Fluorides, such as MgF_2 [135] and LiF [144–146], have also recently demonstrated their ability to be implemented into electron-selective contact materials on c-Si. Most recently, TaO_x was demonstrated to be another suitable electron-selective contact material, resulting already in a first proof-of-concept device in a respectable efficiency of 19.1% [147]. There seems to be an extraordinary diversity of materials usable in hole- or electron-selective contacts on c-Si. At the present point in time, we are only starting to explore the possibilities these new materials might open up for future high-efficiency c-Si solar cells. The parameters of some of the electron-selective contacts discussed are included in Table 1. An attractive approach is to combine electron- and hole-selective materials in one c-Si solar cell, thereby avoiding any dopants. The resulting devices are sometimes denoted 'dopant-free asymmetric heterocontact' (DASH) solar cells. Combining MoO_x as hole-selective layer with TiO_x/LiF stacks as electron-selective contact material and including a thin intrinsic a-Si:H layer at the interfaces led already to efficiencies up to 20.7% [148]. As the research on DASH cells is just at the beginning, much higher efficiencies can be expected in the near future.

5. Discussion and outlook

We have started this review with a brief discussion of the developments that led to the surface passivation schemes applied today in industrially produced dopant-diffused crystalline silicon solar cells, based on the dielectric layers SiO_2, SiN_x and Al_2O_3 as well as stacks thereof. We then discussed the most likely future direction of surface passivation research, which in our view are carrier-selective passivation layers. Whereas the dielectric passivation layers applied in today's commercial cells are insulating and are hence applied only for passivating the non-contacted areas of the silicon surface, carrier-selective passivation layers are intended to provide an effective passivation of non-contacted as well as contacted areas of the solar cell, thereby increasing the efficiency potential. Due to the fact that the carrier-selective layers are implemented in a contact, besides the good passivation properties for minorities, these layers must also provide a good majority carrier transport. Both properties, i.e. suppression of minority-carrier recombination as well as good majority-carrier transport, define the selectivity of the carrier-selective contact, which is an important figure of merit for the assessment and comparison of different types of carrier-selective contacts.

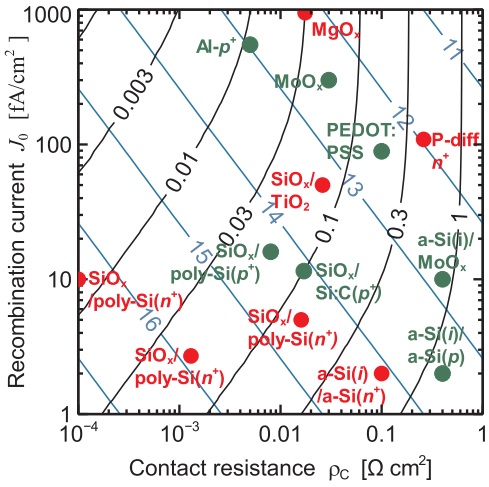

Fig. 10. Data pairs (symbols) of recombination current density parameters J_0 and contact resistances ρ_c for the carrier-selective layers listed in Tables 1, 2. Red symbols are electron-selective layers and green symbols are hole-selective layers. The blue lines are lines of constant selectivity S_{10}. Black lines are lines of constant contact fraction f_{max} that allows maximum efficiency η_{max} assuming that the non-contact area is passivated perfectly. (For interpretation of the references to color in this figure legend, the reader is referred to the web version of this article).

Having discussed various types of carrier-selective contacts in Section 4, we can now compare their selectivities in a single plot. Fig. 10 compiles representative data pairs (red circles for electron-selective, green circles for hole-selective layers) of the recombination currents J_0 and contact resistances ρ_c for the carrier-selective layers listed in Tables 1, 2. The blue lines are lines of constant selectivity S_{10}, whereas the black dashed lines are lines of constant contact fraction f_{max} that allows maximum efficiency η_{max} in an otherwise ideal cell. Both SiO_x/poly-Si(n^+) electron-selective layers, featuring a thermal and a chemical interfacial oxide, respectively, show the largest selectivities S_{10} of around 16. The poly-Si(p^+) layers show only selectivities slightly above 14 and are thus similar to the performance of the classical a-Si:H (i)/a-SiH(p) stacks. The contact area fractions f_{max} of both SiO_x/poly-Si (n^+) layers for maximum efficiency are less than 6%. Thus, the rest of the surface needs to be passivated perfectly, in order to exploit these extraordinarily high selectivities. As such perfect passivation layers with $J_0 = 0$ are not available today, it becomes apparent that – if possible at all – the current SiO_x/poly-Si(n^+) layers should be optimized towards even lower J_0 and moderately higher ρ_c values to exploit their extremely high selectivities in practice.

We are now in the position to evaluate the efficiency potential of various combinations of these contacts systems. From the data of electron-selective contacts in Table 1 and hole-selective contacts in Table 2, we calculate the maximum selectivity $S_{10,e\&h,max}$ using Eq. (18). The current world-record c-Si solar cell with an efficiency of 26.7% features an a-Si:H(i)/a-SiH(p) hole-selective layer and an a-Si:H (i)/a-SiH(n) electron-selective layer. The corresponding combined selectivity is $S_{10,e\&h,max} = 13.2$. In Table 4, this combination is marked with a red box (solid line). We mark all combined selectivity values that are equal or higher than this benchmark selectivity by a blue background. It becomes apparent that the poly-Si layers in combination with

Table 4
Combined selectivity $S_{10,e\&h,max}$ (top left entry), contact area fraction $f_{e,max}$ of electron-selective layer (top right), contact area fraction $f_{h,max}$ of hole-selective layer (bottom left) and maximum efficiency $\eta_{e\&h,max}$ (bottom right) are listed for all contact combinations of Tables 1, 2. These numbers are determined using Eqs. (18), (19), (20), and (13). Selectivities of 13.2 and higher are marked in blue. Efficiencies of 27.5% and above are marked in red. Contact area fractions with 150% < $f_{e,max}$ + $f_{h,max}$ < 250% are marked in grey.

$S_{10,e\&h,max}$	$f_{e,max}$ [%]	Electron-selective contacts													
$f_{h,max}$ [%]	$\eta_{e\&h,max}$ [%]	P-diffused n^+ [57]		a-Si:H(i) /a-Si:H(n) [58]		th-SiO$_x$/ poly-Si(n^+) PECVD [84]		th-SiO$_x$/ poly-Si(n^+) LPCVD [59]		chem-SiO$_x$/ poly-Si(n^+) LPCVD [60]		SiO$_x$/TiO$_2$ [133]		MgO$_x$ [134]	
Hole-selective contacts	Al-doped p^+ [61]	11.7	56	12.8	97	12.8	23	12.9	8.4	13.0	1.2	12.5	12	11.9	4.1
		3.5	24.5	1.3	26.8	1.2	26.9	1.2	27.1	1.1	27.1	1.6	26.3	2.9	24.9
	a-Si:H(i) /a-Si:H(p) [58]	11.8	51	13.2	76	13.3	18	13.5	6.6	13.5	0.90	12.8	9.7	12.0	3.6
		464	24.7	152	27.5	144	27.7	134	27.9	133	28.0	190	26.8	379	25.1
	chem-SiO$_x$/ poly-Si (p^+) [85]	11.9	47	13.6	64	13.8	15	14.2	5.6	14.2	0.80	13.1	8.2	12.1	3.3
		21	24.9	6.4	28.1	6.1	28.3	5.8	28.7	5.7	28.7	8.0	27.3	17	25.4
	chem-SiO$_x$/ Si:C (p^+) [88]	11.9	47	13.5	66	13.7	16	14.0	5.8	14.1	0.8	13.0	8.4	12.1	3.3
		37	24.9	11	28.0	11	28.2	10	28.5	10	28.6	14	27.2	30	25.3
	a-Si:H(i)/ MoO$_x$ [128]	11.7	59	12.6	107	12.7	26	12.8	9.4	12.8	1.3	12.4	13	11.8	4.4
		242	24.4	95.9	26.5	91.5	26.6	85.6	26.8	84.9	26.8	115	26.0	203	24.7
	MoO$_x$ [139]	11.6	67	12.3	139	12.4	34	12.4	12	12.4	1.8	12.2	16	11.7	5.0
		14	24.1	6.2	25.9	6.0	26.0	5.7	26.1	5.6	26.1	7.2	25.5	12	24.4
	PEDOT :PSS [132]	11.6	65	12.4	133	12.4	32	12.5	12	12.5	1.7	12.2	16	11.7	4.9
		47	24.1	21	26.0	20	26.1	19	26.2	19	26.2	25	25.6	40	24.5

one a-Si:H layer and combinations of two poly-Si layers show the highest combined selectivities. Regarding the new materials, the SiO$_x$/TiO$_2$ electron-selective contact in combination with a poly-Si hole-selective layer provides the highest combined selectivity of 13.1.

Using Eq. (13), the maximum efficiency $\eta_{e\&h,max}$ follows from the calculated combined selectivities. For the a-Si:H benchmark case, we calculate a maximum efficiency of $\eta_{e\&h,max}$ = 27.5%. In Table 4, we mark all efficiency potentials of 27.5% or higher with a red background. As expected, these are exactly the same combinations as the blue-marked ones. Note that the efficiency potential of the SiO$_2$/TiO$_x$ electron-selective contact in combination with a poly-Si hole-selective contact is $\eta_{e\&h,max}$ = 27.3% and hence only slightly below the benchmark case. The SiO$_x$/TiO$_2$ contact performs best amongst the new materials discussed in Section 4.2. Poly-Si-based contact systems allow for higher maximum efficiencies than the a-Si:H benchmark case. Among the selection of contact types considered here, the highest efficiency potential is that of SiO$_x$/poly-Si(p^+) hole-selective combined with SiO$_x$/poly-Si(n^+) electron-selective layers. Both these combinations are marked in Table 4 (box framed with red dashed line). The efficiency potential is 28.7% and thus 1%$_{abs}$ higher compared to the a-Si:H benchmark case.

This maximum efficiency can only be reached if the contact fractions $f_{e,max}$ for the electron-selective contact and the area fraction of the hole-selective contact $f_{h,max}$ are close to the optimized values determined with Eqs. (19) and (20), respectively. For example, for the chem-SiO$_x$/poly-Si(p^+) & chem-SiO$_x$/poly-Si(n^+) combination we calculate small contact fractions of $f_{e,max}$ = 0.8% and $f_{h,max}$ = 5.7%. This points to the reason why the poly-Si contacts offer a higher efficiency potential than the a-Si layers: The significantly lower contact resistance of the poly-Si contacts allows for smaller contact areas to reduce the overall recombination. However, our calculation assumes that the non-contacted area is perfectly passivated (i.e. $J_{0,pass}$ = 0). In practice, this is not possible. The poly-Si layers offer $J_{0,e}$ values in the range of 1–10 fA/cm^2 and finding an even better passivation for the non-contacted c-Si surface is quite a challenge. It would thus be advantageous if the optimum contact area fractions $f_{e,max}$ and $f_{h,max}$ could add up to

around 200%, which corresponds to the full front and back surface area. We therefore mark all contact combinations in Table 4 having 150% < ($f_{e,max}$ + $f_{h,max}$) < 250% with a grey background. For these combinations we expect an efficiency potential close to $\eta_{e\&h,max}$ without the need of a third material for passivation of the non-contacted areas. Interestingly, this condition is only fulfilled by five out of the 49 combinations considered, including the new materials MoO_x, PEDOT:PSS and TiO_2. All of these combinations contain at least one a-Si:H-based contact.

Only two of the contact combinations fulfil the condition 150% < ($f_{e,max}$ + $f_{h,max}$) < 250% and do show an efficiency potential of 27.5% or higher. One of these two is the a-Si: H-based benchmark system itself, whereas the other one is the combination of an SiO_x/poly-Si(n^+) electron-selective contact with an a-Si(i)/a-Si:H(p) hole-selective contact. This novel contact combination features an efficiency potential of 27.7% and could thus be interesting to work on experimentally.

We conclude that poly-Si layers do indeed have an exceptional efficiency potential leading to small contact fractions. For exploiting this high potential, a close to perfect passivation of the non-contact area is required. In order to arrive at an efficiency potential estimate without having to assume perfect passivation of the non-contacted surface, we would have to recalculate Table 4 numerically instead of analytically. We leave this to future publications. However, we do not expect significant changes of the calculated maximum efficiency for the most attractive contact combinations identified here which have efficiency potentials above the benchmark case and have 150% < ($f_{e,max}$ + $f_{h,max}$) < 250%. Contact combinations having $f_{e,max}$ + $f_{h,max}$ < 30% could show significantly reduced efficiency potentials when including recombination in the non-contact areas.

The above discussion clearly demonstrated that various combinations of passivating contacts show the potential for very high efficiencies. While poly-Si-based contacts provide the highest overall efficiency potential, the simplicity and elegance of the cell process will also play an important role when selecting the optimal material. Carrier-selective layers which can be deposited on the full-area and therefore do not need any structuring are likely to be the most economic choice. In any case, various carrier-selective layer options for efficiencies > 26% exist and many more are currently developed in the PV labs world-wide. Transferring these new concepts to industrial solar cell production will be the next major challenge.

Acknowledgement

Funding was provided by the State of Lower Saxony.

References

[1] A.G. Aberle, Overview on SiN surface passivation of crystalline silicon solar cells, Sol. Energy Mater. Sol. Cells 65 (2001) 239–248.
[2] R.S. Bonilla, B. Hoex, P. Hamer, P.R. Wilshaw, Dielectric surface passivation for silicon solar cells: a review, Phys. Status Solidi A 1700293 (2017).
[3] R.R. King, R.A. Sinton, R.M. Swanson, Studies of diffused phosphorus emitters: saturation current, surface recombination velocity, and quantum efficiency, IEEE Trans. Electron Dev. 37 (1990) 365–371.
[4] S. W. Glunz, S. Sterk, R. Steeman, W. Warta, J. Knobloch, W. Wettling, Emitter dark saturation currents of high-efficiency solar cells with inverted pyramids, in: Proceedings of the 13th European Photovoltaic Solar Energy Conference., Nice, France, 1995, p. 409.
[5] A. Cuevas, P.A. Basore, G. Giroult-Matlakowski, C. Dubois, Surface recombination velocity of highly doped *n*-type silicon, J. Appl. Phys. 80 (1996) 3370.
[6] R.M. Swanson, S.K. Beckwith, R.A. Crane, W.D. Eades, Y.H. Kwark, R.A. Sinton, S.E. Swirhun, Point-contact silicon solar cells (**ED-31**), IEEE Trans. Electron Dev. (1984) 661–664.
[7] A.W. Blakers, A. Wang, A.M. Milne, J. Zhao, M.A. Green, 22.8% efficient silicon solar cell, Appl. Phys. Lett. 55 (1989) 1363.
[8] S. Sterk, S.W. Glunz, J. Knobloch, W. Wettling, High efficiency (> 22%) Si-solar cells with optimized emitter, in: Proceedings of the 1st World Conference Photovolt. Energy Conv., Hawaii, USA, 1994, pp. 1303–1306.
[9] R. Hezel, Silicon nitride for the improvement of silicon inversion layer solar cells, Solid-State Electron 24 (1981) 863–868.
[10] R. Hezel, K. Jaeger, Low-temperature surface passivation of silicon for solar cells, J. Electrochem. Soc. 136 (1989) 518–523.
[11] A.G. Aberle, T. Lauinger, J. Schmidt, R. Hezel, Injection-level dependent surface recombination velocities at the silicon-plasma silicon nitride interface, Appl. Phys. Lett. 66 (1995) 2828.
[12] C. Leguijt, P. Lölgen, J.A. Eikelboom, A.W. Weeber, F.M. Schuurmans, W.C. Sinke, P.F.A. Alkemade, P.M. Sarro, C.H.M. Maree, L.A. Verhoef, Low-temperature surface passivation for silicon solar cells, Sol. Energy Mater. Sol. Cells 40 (1996) 297–345.
[13] T. Lauinger, J. Schmidt, A.G. Aberle, R. Hezel, Record low surface recombination velocities on 1 Ωcm *p*-silicon using remote plasma silicon nitride passivation, Appl. Phys. Lett 68 (1996), p. 1232.
[14] J. Schmidt, A.G. Aberle, Carrier recombination at silicon-silicon nitride interfaces fabricated by plasma-enhanced chemical vapor deposition, J. Appl. Phys. 85 (1999) 3626.
[15] B. Lenkeit, Elektronische und Strukturelle Eigenschaften von Plasma-Siliziumnitrid zur Oberflächenpassivierung von Siebgedruckten, Bifacialen Silizium-Solarzellen (Ph.D. thesis), University of Hanover, 2002.
[16] J. Schmidt, J.D. Moschner, J. Henze, S. Dauwe, R. Hezel, Recent progress in the surface passivation of silicon solar cells using silicon nitride, in: Proceedings of the 19th European Photovoltaic Solar Energy Conference., Paris, France, 2004, pp. 391–396.
[17] J. Schmidt, M. Kerr, A. Cuevas, Surface passivation of Si solar cells using plasma-enhanced chemical vapor deposited SiN films and thermal SiO_2/plasma SiN stacks, Semicond. Sci. Technol. 16 (2001) 164–170.
[18] M.L. Reed, J.D. Plummer, Chemistry of Si-SiO_2 interface trap annealing, J. Appl. Phys. 63 (1988) 5776–5793.
[19] M.J. Kerr, J. Schmidt, A. Cuevas, J.H. Bultman, Surface recombination velocity of phosphorus-diffused silicon solar cell emitters passivated with plasma enhanced chemical vapor deposited silicon nitride and thermal silicon oxide, J. Appl. Phys. 89 (2001) 3821–3826.
[20] K.R. McIntosh, L.P. Johnson, Recombination at textured silicon surfaces passivated with silicon dioxide, J. Appl. Phys. 105 (2009) 124520.
[21] F. Ye, W. Deng, W. Guo, R. Liu, D. Chen, Y. Chen, Y. Yang, N. Yuan, J. Ding, Z. Feng, P.P. Altermatt, P.J. Verlinden, 22.13% efficient industrial *p*-type mono PERC solar cell, in: Proceedings of the 43rd IEEE Photovoltaic Specialists Conference., Portland, USA, 2016, pp. 3360–3365.
[22] R.R. King, R.M. Swanson, Studies of diffused boron emitters: saturation current, bandgap narrowing, and surface recombination velocity, IEEE Trans. Electron Dev. 38 (1991) 1399–1409.
[23] M.J. Kerr, Surface, Emitter and Bulk Recombination in Silicon and Development of Silicon Nitride Passivated Solar Cells (Ph.D. thesis), Australian National University, 2002.
[24] J. Zhao, J. Schmidt, A. Wang, G. Zhang, B.S. Richards, M.A. Green, Performance instability in n-type PERT silicon solar cells, in: Proceedings of the 3rd World Conference Photovoltaic Solar Energy Conv., Osaka, Japan, 2003, pp. 923–926.
[25] J. Benick, B. Hoex, O. Schultz, S.W. Glunz, Surface passivation of boron diffused emitters for high efficiency solar cells, in: Proceedings of the 33rd IEEE Photovoltaic Specialists Conference, San Diego, CA, USA, IEEE, New York, 2008, ⟨http://dx.doi.org10.1109/PVSC.2008.4922637⟩.
[26] P.P. Altermatt, H. Plagwitz, R. Bock, J. Schmidt, R. Brendel, M.J. Kerr, A. Cuevas, The surface recombination velocity at boron-doped emitters: comparison between various passivation techniques, in: Proceedings of the 21st European Photovoltaic Solar Energy Conference., Dresden, Germany, WIP, Munich, 2006, pp. 647–650.
[27] N.M. Nursam, K.J. Weber, H. Jin, Y. Ren, P. Smith, Investigation of interface properties in oxide passivated boron diffused silicon, Curr. Appl. Phys. 10 (2010) S361–S364.
[28] K. Jaeger, R. Hezel, Conference Rec. 18th IEEE Photov. Specialists Conference, IEEE, New York, 1985, pp. 1752–1753.
[29] B. Hoex, J. Schmidt, R. Bock, P.P. Altermatt, M.C.M. van de Sanden, W.M.M. Kessels, Excellent passivation of highly doped *p*-type Si surfaces by the negative-charge-dielectric Al_2O_3, Appl. Phys. Lett. 91 (2007) 112107.
[30] A. Richter, J. Benick, M. Hermle, Boron emitter passivation with Al_2O_3 and Al_2O_3/SiN_x stacks using ALD Al_2O_3, IEEE J. Photovolt. 3 (2013) 236–245.
[31] J. Schmidt, A. Merkle, R. Bock, P. P. Altermatt, A. Cuevas, N. P. Harder, B. Hoex, M. C. M. van de Sanden, W. M. M. Kessels, R. Brendel, Progress in the surface passivation of silicon solar cells, in: Proceedings of the 23rd European Photovoltaic Solar Energy Conference., Valencia, Spain, WIP, Munich, 2008, pp. 974–981.
[32] P. Saint-Cast, D. Kania, M. Hofmann, J. Benick, J. Rentsch, R. Preu, Very low surface recombination velocity on *p*-type c-Si by high-rate plasma-deposited aluminum oxide, Appl. Phys. Lett. 95 (2009) 151502.
[33] J. Schmidt, F. Werner, B. Veith, D. Zielke, R. Bock, V. Tiba, P. Poodt, F. Roozeboom, A. Li, A. Cuevas, R. Brendel, Industrially relevant Al_2O_3 deposition techniques for the surface passivation of Si solar cells, in: Proceedings of the 25th European Photovoltaic Solar Energy Conference and 5th World Conference Photovolt. Energy Conv., Valencia, Spain, WIP, Munich, 2010, pp. 1130–1133.
[34] S. Bordihn, V. Mertens, J. Cieslak, G. Zimmermanna, R. Lantzsch, J. Scharf, S. Geißler, S. Hörnlein, M. Neuber, S. Laube, A. Dietrich, B. Szramowskia, S. Esefelder, T. Ballmann, B. Eisenhawer, A. Mohr, M. Schaper, K. Petter, J.W. Müller, D. Jeong, R. Hao, T.S. Ravi, Status of industrial back junction *n*-type Si solar cell development, Energy Procedia 92 (2016) 678–683.
[35] N. Wehmeier, B. Lim, A. Nowack, J. Schmidt, T. Dullweber, R. Brendel, 21.0%-efficient co-diffused screen-printed *n*-type silicon solar cell with rear-side boron emitter, Phys. Status Solidi RRL 10 (2016) 148–152.
[36] J. Engelhardt, A. Frey, S. Gloger, G. Hahn, B. Terheiden, Passivating boron silicate glasses for co-diffused high-efficiency *n*-type silicon solar cell application, Appl.

Phys. Lett. 107 (2015) 042102.
[37] T. Dullweber, N. Wehmeier, A. Nowack, T. Brendemühl, S. Kajari-Schröder, R. Brendel, Industrial bifacial *n*-type silicon solar cells applying a boron co-diffused rear emitter and an aluminum rear finger grid, Phys. Status Solidi A 213 (2016) 30463052.
[38] N. Wehmeier, A. Nowack, B. Lim, T. Brendemühl, S. Kajari-Schröder, J. Schmidt, R. Brendel, T. Dullweber, 21.0%-efficient screen-printed *n*-PERT back-junction silicon solar cell with plasma-deposited boron diffusion source, Sol. Energy Mater. Sol. Cells 158 (2016) 50.
[39] T. Dullweber, J. Schmidt, Industrial silicon solar cells applying the passivated emitter and rear cell (PERC) concept – a review, IEEE J. Photovolt. 6 (2016) 1366.
[40] A. Hübner, A.G. Aberle, R. Hezel, Novel cost-effective bifacial silicon solar cells with 19.4% front and 18.1% rear efficiency, Appl. Phys. Lett. 70 (1997) 1008–1010.
[41] S. Dauwe, L. Mittelstädt, A. Metz, R. Hezel, Experimental evidence of parasitic shunting in silicon nitride rear surface passivated solar cells, Prog. Photovolt. Res. Appl. 10 (2002) 271–278.
[42] G. Agostinelli, A. Delabie, P. Vitanov, Z. Alexieva, H.F.W. Dekkers, S. De Wolf, G. Beaucarne, Very low surface recombination velocities on *p*-type silicon wafers passivated with a dielectric with fixed negative charge, Sol. Energy Mater. Sol. Cells 90 (2006) 3438–3443.
[43] B. Hoex, S.B.S. Heil, E. Langereis, M.C.M. van de Sanden, W.M.M. Kessels, Ultralow surface recombination of c-Si substrates passivated by plasma-assisted atomic layer deposited Al_2O_3 (042112/), Appl. Phys. Lett. 89 (2006) 1–3 (042112/).
[44] S. Miyajima, J. Irikawa, A. Yamada, M. Konagai, Hydrogenated aluminum oxide films deposited by plasma enhanced chemical vapor deposition for passivation of *p*-type crystalline silicon, in: Proceedings of the 23rd European Photovoltaic Solar Energy Conference, Valencia, Spain, 2008, pp. 1029–1032.
[45] T.T. Li, A. Cuevas, Effective surface passivation of crystalline silicon by rf sputtered aluminum oxide, Phys. Status Solidi RRL 3 (2009) 160–162.
[46] J. Schmidt, B. Veith, R. Brendel, Effective surface passivation of crystalline silicon using ultrathin Al_2O_3 films and Al_2O_3/SiN_x stacks, Phys. Status Solidi RRL 3 (2009) 287–289.
[47] G. Dingemans, R. Seguin, P. Engelhart, M.C.M. van de Sanden, W.M.M. Kessels, Silicon surface passivation by ultrathin Al_2O_3 films synthesized by thermal and plasma atomic layer deposition, Phys. Status Solidi RRL 4 (2010) 10–12.
[48] J. Schmidt, F. Werner, B. Veith, D. Zielke, R. Bock, V. Tiba, P. Poodt, F. Roozeboom, A. Li, A. Cuevas, R. Brendel, Industrially relevant Al_2O_3 deposition techniques for the surface passivation of Si solar cells, in: Proceedings of the 25th European Photovoltaic Solar Energy Conference and 5th World Conference Photovolt. Energy Conv., Valencia, Spain, 2010, pp. 1130–1133.
[49] J. Schmidt, A. Merkle, R. Bock, P. P. Altermatt, A. Cuevas, N. P. Harder, B. Hoex, M. C. M. van de Sanden, W. M. M. Kessels, R. Brendel, Progress in the surface passivation of silicon solar cells, Proceedings of the 23rd European Photovoltaic Solar Energy Conference, Valencia, Spain, WIP, Munich, 2008, 974–981.
[50] G. Dingemans, M.C.M. van de Sanden, W.M.M. Kessels, Influence of the deposition temperature on the c-Si surface passivation by Al_2O_3 films synthesized by ALD and PECVD, Electrochem. Solid-State Lett. 13 (2010) H76–H79.
[51] B. Veith, T. Dullweber, M. Siebert, C. Kranz, F. Werner, N.-P. Harder, J. Schmidt, B.F.P. Roos, T. Dippell, R. Brendel, Comparison of ICP-AlO_x and ALD-Al_2O_3 layers for the rear surface passivation of c-Si Solar cells, Energy Procedia 27 (2012) 379–384.
[52] L.E. Black, T. Allen, A. Cuevas, K.R. McIntosh, B. Veith, J. Schmidt, Thermal stability of surface passivation by APCVD Al_2O_3, Sol. Energy Mater. Sol. Cells 120 (2014) 339–345.
[53] J. Schmidt, A. Merkle, R. Brendel, M.C.M. van de Sanden, W.M.M. Kessels, Surface passivation of high-efficiency silicon solar cells by atomic-layer-deposited Al_2O_3, Prog. Photovolt.: Res. Appl. 16 (2008) 461–466.
[54] T. Dullweber, C. Kranz, B. Beier, B. Veith, J. Schmidt, B.F.P. Roos, O. Hohn, T. Dippell, R. Brendel, Inductively coupled plasma chemical vapour deposited AlO_x/SiN_y layer stacks for applications in high-efficiency industrial-type silicon solar cells, Sol. Energy Mater. Sol. Cells 112 (2013) 196–201.
[55] B. Veith, F. Werner, D. Zielke, R. Brendel, J. Schmidt, Comparison of the thermal stability of single Al_2O_3 layers and Al_2O_3/SiN_x stacks for the surface passivation of silicon, Energy Procedia 8 (2011) 307–312.
[56] H. Hannebauer, T. Dullweber, U. Baumann, T. Falcon, R. Brendel, 21.2%-efficient fine-line-printed PERC solar cell with 5 busbar front grid, Phys. Status Solidi – RRL 8 (2014) 675–679.
[57] R. Brendel, R. Peibst, Contact selectivity and efficiency in crystalline silicon photovoltaics, IEEE J. Photovolt. 6 (2016) 1413–1420.
[58] S.Y. Herasimenka, W.J. Dauksher, S.G. Bowden, > 750 mV open circuit voltage measured on 50 μm thick silicon heterojunction solar cell, Appl. Phys. Lett. 103 (2013) 053511.
[59] M. Rienäcker, M. Bossmeyer, A. Merkle, U. Römer, F. Haase, J. Krügener, R. Brendel, R. Peibst, Junction resistivity of carrier-selective polysilicon on oxide junctions and its impact on solar cell performance, IEEE J. Photovolt. 7 (2017) 11.
[60] G. Kökbudak, R. Müller, F. Feldmann, A. Fell, R. Turan, S.W. Glunz, in: Proceedings 33rd European Photovolt. Solar Energy Conference, WIP, Munich, 2017, pp. 242–246.
[61] R. Brendel, T. Dullweber, R. Peibst, C. Kranz, A. Merkle, D. Walter, Breakdown of the efficiency gap to 29% based on experimental input data and modeling, Prog. Photovolt.: Res. Appl. 24 (2016) 1475–1486.
[62] P. Koswatta, M. Boccard, Z. Holman, Carrier-selective contacts in silicon solar cells, in: Proceedings 42nd IEEE Photovolt. Spec. Conference., New Orleans, USA, IEEE, New York, 2015), pp. 1–4.
[63] R. Brendel, R. Peibst, Contact selectivity and efficiency in crystalline silicon photovoltaics, IEEE J. Photovolt. 6 (2016) 1413–1420.
[64] R. Brendel, M. Rienäcker, R. Peibst, A quantitative measure for the carrier selectivity of contacts to solar cells, in: Proceedings 32nd European Photovolt. Solar Energy Conference., Munich, Germany, WIP, Munich, 2016, pp. 447–451.
[65] K. Yoshikawa, W. Yoshida, T. Irie, H. Kawasaki, K. Konishi, H. Ishibashi, T. Asatani, D. Adachi, M. Kanematsu, H. Uzu, K. Yamamoto, Exceeding conversion efficiency of 26% by heterojunction interdigitated back contact solar cell with thin film Si technology, Sol. Energy Mater. Sol. Cells 173 (2017) 37–42.
[66] M.A. Green, Y. Hishikawa, W. Warta, E.D. Dunlop, D.H. Levi, J. Hohl-Ebinger, A. Ho-Baillie, Solar cell efficiency tables (version 50), Prog. Photovolt. Res. Appl. 25 (2017) 668–676.
[67] S. DeWolf, A. Descoeudres, Z.C. Holman, C. Ballif, High-efficiency silicon heterojunction solar cells: a review, Green 2 (2012) 7–24.
[68] J. Graul, A. Glasl, H. Murrmann, Ion implanted bipolar high performance transistors with polysil emitter, in: Proceedings of International Electron Dev. Meeting, Washington DC, USA, IEEE, New York, 1975, pp. 450–454.
[69] J. Graul, A. Glasl, H. Murrmann, High-performance transistors with arsenic-implanted polysil emitters, IEEE J. Solid-State Circ. 11 (1976) 491–495.
[70] I.R.C. Post, P. Ashburn, G.R. Wolstenholme, Polysilicon emitters for bipolar transistors: a review and re-evaluation of theory and experiment, IEEE Trans. Electron Dev. 39 (1992) 1717–1731.
[71] J. Fossum, M. Shibib, A minority-carrier transport model for polysilicon contacts to silicon bipolar devices, including solar cells, in: Proceedings of International Electron Dev. Meeting, Washington DC, USA, IEEE, New York, 1980, pp. 280–283.
[72] F. Lindholm, A. Neugroschel, M. Arienzo, P. Iles, Heavily doped polysilicon-contact solar cells, IEEE Electron Dev. Lett. 6 (1985) 363–365.
[73] E. Yablonovitch, T. Gmitter, R.M. Swanson, Y.H. Kwark, A 720 mV open circuit voltage SiO_x:c-Si: SiO_x double heterostructure solar cell, Appl. Phys. Lett. 47 (1985) 1211–1213.
[74] N.G. Tarr, A polysilicon emitter solar cell, IEEE Electron Dev. Lett. 6 (1985) 655–658.
[75] J. Y. Gan and R. M. Swanson, Polysilicon emitters for silicon concentrator solar cells, in: Proceedings 21st IEEE Photovolt. Spec. Conference, IEEE, New York, 1990, pp. 245–250.
[76] U. Römer, R. Peibst, T. Ohrdes, B. Lim, J. Krügener, T. Wietler, R. Brendel, Ion implantation for poly-Si passivated back-junction back-contacted solar cells, IEEE J. Photovolt. 5 (2015) 507–514.
[77] A. Moldovan, F. Feldmann, M. Zimmer, J. Rentsch, J. Benick, M. Hermle, Tunnel oxide passivated carrier-selective contacts based on ultra-thin SiO_2 layers, Sol. Energy Mater. Sol. Cells 142 (2015) 123–127.
[78] U. Römer, R. Peibst, T. Ohrdes, B. Lim, J. Krügener, E. Bugiel, T. Wietler, R. Brendel, Recombination behaviour and contact resistance of n^+ and p^+ polycrystalline Si/mono-crystalline Si junctions, Sol. Energy Mater. Sol. Cells 131 (2014) 85–91.
[79] F. Feldmann, M. Bivour, C. Reichel, M. Hermle, S.W. Glunz, Passivated rear contacts for high-efficiency n-type Si solar cells providing high interface passivation quality and excellent transport characteristics, Sol. Energy Mater. Sol. Cells 120 (2014) 270–274.
[80] R. Peibst, Y. Larionova, S. Reiter, M. Turcu, R. Brendel, D. Tetzlaff, J. Krügener, T. Wietler, U. Höhne, J. Kähler, H. Mehlich, S. Frigge, Implementation of n^+ and p^+ POLO junctions on front and rear side of double-side contacted industrial silicon solar cells, in: Proceedings 32nd Europ. Photovolt. Sol. Energy Conference, Munich, Germany, WIP, Munich, 2016, pp. 323–327.
[81] S. Choi, K.H. Min, M.S. Jeon, J.I. Lee, M.G. Kang, H.-E. Son, Y. Kang, H.-S. Lee, D. Kim, K.-H. Kim, Structural evolution of tunneling oxide passivating contact upon thermal annealing, Sci. Rep. 7 (2017) 12853.
[82] M.K. Stodolny, M. Lenes, Y. Wu, G.J.M. Janssen, I.G. Romijn, J.R.M. Luchies, L.J. Geerligs, N-type polysilicon passivating contact for industrial bifacial n-type solar cells, Sol. Energy Mater. Sol. Cells 158 (2016) 24–28.
[83] S. Mack, J. Schube, T. Fellmeth, F. Feldmann, M. Lenes, J.-M. Luchies, Metallisation of boron-doped polysilicon layers by screen printed silver pastes, Phys. Status Solidi RRL 1700334 (2017).
[84] D. Yan, A. Cuevas, J. Bullock, Y. Wan, C. Samundsett, Phosphorus-diffused polysilicon contacts for solar cells, Sol. Energy Mater. Sol. Cells 142 (2015) 75–82.
[85] D. Yan, A. Cuevas, Y. Wan, J. Bullock, Passivating contacts for silicon solar cells based on boron-diffused recrystallized amorphous silicon and thin dielectric interlayers, Sol. Energy Mater. Sol. 152 (2016) 73–79.
[86] B. Nemeth, D.L. Young, M.R. Page, V. LaSalvia, S. Johnston, R. Reedy, P. Stradins, Polycrystalline silicon passivated tunneling contacts for high efficiency silicon solar cells, J. Mater. Res 31 (2016) 671–681.
[87] Y. Tao, V. Upadhyaya, C.-W. Chen, A. Payne, E.L. Chang, A. Upadhyaya, A. Rohatgi, Large area tunnel oxide passivated rear contact *n*-type Si solar cells with 21.2% efficiency, Prog. Photovolt.: Res. Appl. 24 (2016) 830–835.
[88] G. Nogay, J. Stuckelberger, P. Wyss, E. Rucavado, C. Allebé, T. Koida, M. Morales-Masis, M. Despeisse, F.-J. Haug, P. Löper, C. Ballif, Interplay of annealing temperature and doping in hole selective rear contacts based on silicon-rich silicon-carbide thin films, Sol. Energy Mater. Sol. Cells 173 (2017) 18–24.
[89] J. Stuckelberger, G. Nogay, P. Wyss, Q. Jeangros, C. Allebé, F. Debrot, X. Niquille, M. Ledinsky, A. Fejfar, M. Despeisse, F.-J. Haug, P. Löper, C. Ballif, Passivating electron contact based on highly crystalline nanostructured silicon oxide layers for silicon solar cells, Sol. Energy Mater. Sol. Cells 158 (2016) 2–10.
[90] Y.H. Kwark, R.M. Swanson, N-type SIPOS and poly-Si emitters, Solid-State Electron 30 (1987) 1121–1125.
[91] P. Borden, L. Xu, B. McDugall, C.P. Chang, P. Pysch, P. Voisin, S.W. Glunz, Polysilicon tunnel junctions as alternates to diffused junctions, in: Proceedings

23rd Europ. Photovolt. Sol. Energy Conference, WIP, Munich, 2008, pp. 1149–1152.
[92] F. Feldmann, M. Bivour, C. Reichel, M. Hermle, S.W. Glunz, A passivated rear contact for high-efficiency *n*-type Si solar cells enabling high V_{oc}s and *FF* > 82%, in: Proceedings 28th Europ. Photovolt. Solar Energy Conference, 2013, pp. 988–992.
[93] R. Brendel, T. Dullweber, R. Gogolin, H. Hannebauer, N.-P. Harder, J. Hensen, S. Kajari-Schröder, R. Peibst, J.H. Petermann, U. Römer, J. Schmidt, H. Schulte-Huxel, V. Steckenreiter, Recent progress and options for future crystalline silicon solar cells, in: Proceedings 28th Europ. Photovolt. Solar Energy Conference, 2013, pp. 676–690.
[94] R. Peibst, U. Römer, Y. Larionova, M. Rienäcker, A. Merkle, N. Folchert, S. Reiter, M. Turcu, B. Min, J. Krügener, D. Tetzlaff, E. Bugiel, T. Wietler, R. Brendel, Working principle of carrier selective poly-Si/c-Si junctions: is tunneling the whole story? Sol. Energy Mater. Sol. Cells 158 (2016) 60–67.
[95] R. Peibst, U. Römer, K.R. Hofmann, B. Lim, T.F. Wietler, J. Krügener, N.-P. Harder, R. Brendel, A simple model describing the symmetric *I–V* characteristics of *p* polycrystalline Si/*n* monocrystalline Si, and *n* polycrystalline Si/*p* monocrystalline Si junctions, IEEE J. Photovolt. 4 (2014) 841–850.
[96] G.J.M. Janssen, M.K. Stodolny, I.G. Romijn, L.J. Geerligs, The role of the oxide in the carrier selectivity of metal/poly-Si/oxide contacts to silicon wafers, in: Proceedings 33rd Europ. Photovolt. Sol. En. Conference., Amsterdam, The Netherlands, 2017, pp. 256–261.
[97] K. Lancaster, S. Großer, F. Feldmann, V. Naumann, C. Hagendorf, Study of pinhole conductivity at passivated carrier-selected contacts of silicon solar cells, Energy Procedia 92 (2016) 116–121.
[98] D. Tetzlaff, J. Krügener, Y. Larionova, S. Reiter, M. Turcu, R. Peibst, U. Höhne, J.-D. Kähler, T. Wietler, Evolution of oxide disruptions: The (w)hole story about passivating contacts, in: Proceedings 43rd IEEE Photovolt. Spec. Conference., Portland, OR, USA, IEEE, New York, 2016, pp. 221–224.
[99] D. Tetzlaff, J. Krügener, Y. Larionova, S. Reiter, M. Turcu, F. Haase, R. Brendel, R. Peibst, U. Höhne, J.D. Kähler, T.F. Wietler, A simple method for pinhole detection in carrier selective POLO-junctions for high efficiency silicon solar cells, Sol. Energy Mater. Sol. Cells 173 (2017) 106–110.
[100] T.F. Wietler, D. Tetzlaff, J. Krügener, M. Rienäcker, F. Haase, Y. Larionova, R. Brendel, R. Peibst, Pinhole density and contact resistivity of carrier selective junctions with polycrystalline silicon on oxide, Appl. Phys. Lett. 110 (2017) 253902.
[101] P.P. Altermatt, J.O. Schumacher, A. Cuevas, M.J. Kerr, S.W. Glunz, R.R. King, G. Heiser, A. Schenk, Numerical modeling of highly doped Si:P emitters based on Fermi–Dirac statistics and self-consistent material parameters, J. Appl. Phys. 92 (2002) 3187–3197.
[102] B.E. Deal, M. Sklar, A.S. Grove, E.H. Snow, Characteristics of the surface-state charge (Q_{ss}) of thermally oxidized silicon, J. Electrochem. Soc. 114 (1967) 266–274.
[103] A. G. Aberle, *Advanced surface passivation and analysis*, University of New South Wales, Chapter 4.2.2 (2009).
[104] D.L. Young, W. Nemeth, V. LaSalvia, R. Reedy, S. Essig, N. Bateman, P. Stradins, Interdigitated back passivated contact (IBPC) solar cells formed by ion implantation, IEEE J. Photovolt. 6 (2016) 41.
[105] F. Haase, F. Kiefer, S. Schäfer, C. Kruse, J. Krügener, R. Brendel, R. Peibst, Interdigitated back contact solar cells with polycrystalline silicon on oxide passivating contacts for both polarities, Jpn. J. Appl. Phys. 56 (2017) 08MB15.
[106] Y. Larionova, M. Turcu, S. Reiter, R. Brendel, D. Tetzlaff, J. Krügener, T. Wietler, U. Höhne, J.-D. Kähler, R. Peibst, On the recombination behavior of p-type polysilicon on oxide junctions deposited by different methods on textured and planar surfaces, Phys. Stat. Sol. A 1700058 (2017).
[107] J.A. Cooper Jr., R.J. Schwartz, Electrical characteristics of the SiO_2/Si interface near midgap and in weak inversion, Solid-State Electron 17 (1974) 641–654.
[108] Y. Kato, H. Takao, K. Sawada, M. Ishida, Improvement of metal-oxide semiconductor interface characteristics in complementary metal-oxide semiconductor on Si(111) by combination of fluorine implantation and long-time hydrogen annealing, Jpn. J. Appl. Phys. 45 (2006) L108.
[109] F. Feldmann, R. Müller, C. Reichel, M. Hermle, Ion implantation into amorphous Si layers to form carrier-selective contacts for Si solar cells, Phys. Status Solidi RRL 8 (2014) 767–770.
[110] A.G. Aberle, S.W. Glunz, A.W. Stephens, M.A. Green, High-efficient Si solar cells: Si-SiO_2 interface parameters and their impact on device performance, J. Appl. Phys. 71 (1992) 4422.
[111] M. Dutoit, F. Sollberger, Lateral polysilicon *p-n* diodes, J. Electrochem. Soc. 125 (1978) 1648–1651.
[112] A.K. Ghosh, C. Fishman, T. Feng, Theory of the electrical and photovoltaic properties of polycrystalline silicon, J. Appl. Phys. 51 (1980) 446–454.
[113] K. Preston, P. Dong, B. Schmidt, M. Lipson, High-speed all-optical modulation using polycrystalline silicon microring resonators, Appl. Phys. Lett. 92 (2008) 151104.
[114] D.L. Young, W. Nemeth, V. LaSalvia, M.R. Page, S. Theingi, J. Aguiar, B.G. Lee, P. Stradins, Low-cost plasma immersion ion implantation doping for interdigitated back passivated contact (IBPC) solar cells, Sol. Energy Mater. Sol. Cells 158 (2016) 68–76.
[115] U. Römer, Polycrystalline Silicon / Monocrystalline Silicon Junctions and Their Application as Passivated Contacts for Si Solar Cells (Ph.D. thesis), Leibniz Universität Hannover, 2016.
[116] A. Richter, J. Benick, R. Müller, F. Feldmann, C. Reichel, M. Hermle, S.W. Glunz, Tunnel oxide passivating electron contacts as full area rear emitter of high efficiency p-type silicon solar cells, Prog. Photovolt. Res. Appl. (2017) 1–8, https://doi.org/10.1002/pip.2960.
[117] Y. Larionova, R. Peibst, M. Turcu, S. Reiter, R. Brendel, D. Tetzlaff, J. Krügener, T. Wietler, U. Höhne, J.-D. Kähler, Optimization of p^+ poly-Si/c-Si junctions on wet-chemically grown interfacial oxides and on different wafer morphologies, in: Proceedings of the 32nd European Photovoltaic Solar Energy Conference., Munich, Germany, WIP, Munich, 2016, pp. 452–455.
[118] D.L. Young, B.G. Lee, D. Fogel, W. Nemeth, V. LaSalvia, S. Theingi, M. Page, M. Young, C. Perkins, P. Stradins, Gallium-doped poly-Si:Ga/SiO_2 passivated emitters to n-Cz wafers with iV_{oc} > 730 mV, IEEE J. Photovolt. 7 (2017) 1640.
[119] J. Meyer, S. Hamwi, M. Kröger, W. Kowalsky, T. Riedl, A. Kahn, Transition metal oxides for organic electronics: energetics, device physics and applications, Adv. Mater. 24 (2012) 5408–5427.
[120] A. Elschner, S. Kirchmeyer, W. Lövenich, U. Merker, and K. Reuter, PEDOT: Principles and Applications of an Intrinsically Conductive Polymer, CRC Press, Boca Raton, FL, 2011.
[121] S. Avasthi, S. Lee, Y.L. Loo, J.C. Sturm, Role of majority and minority carrier barriers silicon/organic hybrid heterojunction solar cells, Adv. Mater. 23 (2011) 5762–5766.
[122] A. Cuevas, T. Allen, J. Bullock, Y. Wand, D. Yan, X. Zhang, Skin care for healthy silicon solar cells, in: Proceedings of the 42nd IEEE Photovolt. Spec. Conference., New Orleans, LA, USA, IEEE, New York, 2015, pp. 1–6.
[123] S. Heo, E. Cho, H. Lee, G.S. Park, H.J. Kang, T. Nagatomi, P. Choi, B.D. Choi, Band gap and defect states of MgO thin films investigated using reflection electron energy loss spectroscopy, AIP Adv. 5 (2015) 077167.
[124] L.G. Gerling, G. Masmitja, C. Voz, P. Ortega, J. Puigdollers, R. Alcubilla, Back junction n-type silicon heterojunction solar cells with V_2O_5 hole-selective contact, Energy Procedia 92 (2016) 633–637.
[125] L.G. Gerling, S. Mahato, A. Morales-Vilches, G. Masmitja, P. Ortega, C. Voz, R. Alcubilla, J. Puigdollers, Transition metal oxides as hole-selective contacts in silicon heterojunction solar cells, Sol. Energy Mater. Sol. Cells 145 (2016) 109–115.
[126] M. Bivour, J. Temmler, F. Zähringer, S. Glunz, M. Hermle, High work function metal oxides for the hole contact of silicon solar cells, in: Proceedings 43rd IEEE Photovolt. Spec. Conference., Portland, OR, USA, IEEE, New York, 2016, pp. 215–220.
[127] C. Battaglia, S.M. Nicolas, S. De Wolf, X. Yin, M. Zheng, C. Ballif, A. Javey, Silicon heterojunction solar cell with passivated hole selective MoO_x contact, Appl. Phys. Lett. 104 (2014) 113902.
[128] J. Geissbühler, J. Werner, S.M. Nicolas, L. Barraud, A. Hessler-Wyser, M. Despeisse, S. Nicolay, A. Tomasi, B. Niesen, S. De Wolf, C. Ballif, 22.5% efficient silicon heterojunction solar cell with molybdenum oxide hole collector, Appl. Phys. Lett. 107 (2015) 081601.
[129] M. Bivour, J. Temmler, H. Steinkemper, M. Hermle, Molybdenum and tungsten oxide: high work function wide band gap contact materials for hole selective contacts of silicon solar cells, Sol. Energy Mater. Sol. Cells 142 (2015) 34–41.
[130] L. He, C. Jiang, H. Wang, D. Lai, und Rusli, High efficiency planar Si/organic heterojunction hybrid solar cells, Appl. Phys. Lett. 100 (2012) 073503.
[131] J. Schmidt, V. Titova, D. Zielke, Organic-silicon heterojunction solar cells: open-circuit voltage potential and stability, Appl. Phys. Lett. 103 (2013) 183901.
[132] D. Zielke, C. Niehaves, W. Lövenich, A. Elschner, M. Hörteis, J. Schmidt, Organic-silicon solar cells exceeding 20% efficiency, Energy Procedia 77 (2015) 331–339.
[133] X. Yang, K. Weber, Z. Hameiri, S. De Wolf, Industrially feasible, dopant-free, carrier-selective contacts for high-efficiency silicon solar cells, Prog. Photovolt.: Res. Appl. 25 (2017) 896–904.
[134] Y. Wan, C. Samundsett, J. Bullock, M. Hettick, T. Allen, D. Yan, J. Peng, Y. Wu, A. Javey, A. Cuevas, Conductive and stable magnesium oxide electron-selective contacts for efficient silicon solar cells, Adv. Energy Mater. 1601863 (2016).
[135] Y. Wan, C. Samundsett, J. Bullock, T. Allen, M. Hettick, D. Yan, P.T. Zheng, X.Y. Zhang, J. Cui, J. McKeon, A. Javey, A. Cuevas, Magnesium fluoride electron-selective contacts for crystalline silicon solar cells, ACS Appl. Mater. Interfaces 8 (2016) 14671–14677.
[136] Y.F. Zhang, W. Cui, Y.W.F.S. Zu, L.S. Liao, S.T. Lee, B.Q. Sun, High efficiency hybrid PEDOT:PSS/nanostructured silicon Schottky junction solar cells by doping-free rear contact, Energy Environ. Sci. 8 (2015) 297–302.
[137] M. Tanaka, M. Taguchi, T. Matsuyama, T. Sawada, S. Tsuda, S. Nakano, H. Hanafusa, Y. Kuwanoe, Development of new a-Si/c-Si heterojunction solar cells: ACJ-HITacj (artificially constructed junction heterojunction with intrinsic thin-layer), Jpn. J. Appl. Phys. 31 (1992) 3518.
[138] R. Gogolin, M. Turcu, R. Ferré, J. Clemens, N.-P. Harder, R. Brendel, J. Schmidt, Analysis of series resistance losses in a-Si: h/c-si heterojunction solar cells, IEEE J. Photovolt. 4 (2014) 1169–1176.
[139] J. Bullock, A. Cuevas, T. Allen, C. Battaglia, Molybdenum oxide MoO_x: a versatile hole contact for silicon solar cells, Appl. Phys. Lett. 105 (2014) 232109.
[140] D. Zielke, A. Pazidis, F. Werner, J. Schmidt, Organic-silicon heterojunction solar cells on n-type silicon wafers: the BackPEDOT concept, Sol. Energy Mater. Sol. Cells 131 (2014) 110–116.
[141] R. Gogolin, D. Zielke, W. Lövenich, R. Sauer, J. Schmidt, Silicon hetero-junction solar cells combining an a-Si:H electron-collector with a PEDOT:PSS hole-collector, Energy Procedia 92 (2016) 638.
[142] J. Schmidt, D. Zielke, R. Gogolin, R. Sauer, and W. Lövenich, Recent advances in polymer/silicon heterojunction solar cells, in: Proceedings of the 32nd European Photovoltaic Solar Energy Conference, Munich, Germany, WIP, Munich, 2016, p. 85–88.
[143] V. Titova, B. Veith-Wolf, D. Startsev, J. Schmidt, Effective passivation of crystalline silicon surfaces by ultrathin atomic-layer-deposited TiO_x layers, Energy Procedia 124 (2017) 441.

[144] Y.F. Zhang, R.Y. Liu, S.T. Lee, B.Q. Sun, The role of a LiF layer on the performance of PEDOT:PSS/Si organic-inorganic hybrid solar cells, Appl. Phys. Lett. 104 (2014) 083514.
[145] J. Bullock, P. Zheng, Q. Jeangros, M. Tosun, M. Hettick, C.M. Sutter-Fella, Y. Wan, T. Allen, D. Yan, D. Macdonald, S. De Wolf, A. Hessler-Wyser, A. Cuevas, A. Javey, Lithium fluoride based electron contacts for high efficiency n-type crystalline silicon solar cells, Adv. Energy Mater. 6 (2016) 1600241.
[146] J. Bullock, M. Hettick, J. Geissbühler, A.J. Ong, T. Allen, C.M. Sutter-Fella, T. Chen, H. Ota, E.W. Schaler, S. De Wolf, C. Ballif, A. Cuevas, A. Javey, Efficient silicon solar cells with dopant-free asymmetric heterocontacts, Nat. Energy 1 (2016) 15031.
[147] Y. Wan, S.K. Karuturi, C. Samundsett, J. Bullock, M. Hettick, D. Yan, J. Peng, P.R. Narangari, S. Mokkapati, H.H. Tan, C. Jagadish, A. Javey, A. Cuevas, Tantalum oxide electron-selective heterocontacts for silicon photovoltaics and photoelectrochemical water reduction, ACS Energy Lett. 3 (2018) 125–131.
[148] J. Bullock, Y. Wan, Z. Xu, S. Essig, M. Hettick, H. Wang, W. Ji, M. Boccard, A. Cuevas, C. Ballif, A. Javey, ACS Energy Lett. 3 (2018) 508–513.